

Satellite observations of the Northeast Pacific Ocean

Emmanuel Devred, Melanie Hardy, and Charles Hannah

Fisheries and Oceans Canada
Bedford Institute of Oceanography
P.O. Box 1006
Dartmouth, Nova Scotia
Canada, B2Y 4A2

2021

Canadian Technical Report of
Hydrography and Ocean Sciences 335



Fisheries and Oceans
Canada

Pêches et Océans
Canada

Canada

Canadian Technical Report of Hydrography and Ocean Sciences

Technical reports contain scientific and technical information of a type that represents a contribution to existing knowledge but which is not normally found in the primary literature. The subject matter is generally related to programs and interests of the Oceans and Science sectors of Fisheries and Oceans Canada.

Technical reports may be cited as full publications. The correct citation appears above the abstract of each report. Each report is abstracted in the data base *Aquatic Sciences and Fisheries Abstracts*.

Technical reports are produced regionally but are numbered nationally. Requests for individual reports will be filled by the issuing establishment listed on the front cover and title page.

Regional and headquarters establishments of Ocean Science and Surveys ceased publication of their various report series as of December 1981. A complete listing of these publications and the last number issued under each title are published in the *Canadian Journal of Fisheries and Aquatic Sciences*, Volume 38: Index to Publications 1981. The current series began with Report Number 1 in January 1982.

Rapport technique canadien sur l'hydrographie et les sciences océaniques

Les rapports techniques contiennent des renseignements scientifiques et techniques qui constituent une contribution aux connaissances actuelles mais que l'on ne trouve pas normalement dans les revues scientifiques. Le sujet est généralement rattaché aux programmes et intérêts des secteurs des Océans et des Sciences de Pêches et Océans Canada.

Les rapports techniques peuvent être cités comme des publications à part entière. Le titre exact figure au-dessus du résumé de chaque rapport. Les rapports techniques sont résumés dans la base de données *Résumés des sciences aquatiques et halieutiques*.

Les rapports techniques sont produits à l'échelon régional, mais numérotés à l'échelon national. Les demandes de rapports seront satisfaites par l'établissement auteur dont le nom figure sur la couverture et la page de titre.

Les établissements de l'ancien secteur des Sciences et Levés océaniques dans les régions et à l'administration centrale ont cessé de publier leurs diverses séries de rapports en décembre 1981. Vous trouverez dans l'index des publications du volume 38 du *Journal canadien des sciences halieutiques et aquatiques*, la liste de ces publications ainsi que le dernier numéro paru dans chaque catégorie. La nouvelle série a commencé avec la publication du rapport numéro 1 en janvier 1982.

Canadian Technical Report of
Hydrography and Ocean Sciences 335

2021

SATELLITE OBSERVATIONS OF THE NORTHEAST PACIFIC OCEAN

by

Emmanuel Devred, Melanie Hardy, and Charles Hannah

Ocean and Ecosystem Sciences Division,
Fisheries and Oceans Canada
Bedford Institute of Oceanography
P.O. Box 1006
Dartmouth, Nova Scotia
Canada, B2Y 4A2

©Her Majesty the Queen in Right of Canada, 2021
Cat. No. Fs97-18/335E-PDF ISBN 978-0-660-37174-0 ISSN 1488-5417

Correct Citation for this publication:

Devred, E., Hardy, M., and Hannah, C. 2021. Satellite observations of the Northeast Pacific Ocean.
Can. Tech. Rep. Hydrogr. Ocean Sci. 335: vii + 46 p.

CONTENTS

List of Tables	iv
List of Figures	v
ABSTRACT	vi
RÉSUMÉ	vii
1 Introduction	1
2 Data and Methods	2
2.1 Region of Interest	2
2.2 Data	2
2.2.1 <i>In situ</i> Temperature	2
2.2.2 Satellite Data	4
2.3 Methods	5
2.3.1 Daily and Monthly Mean	5
2.3.2 Temporal and Spatial Cover	5
2.3.3 Seven-day Climatology	5
2.3.4 Environmental indices	6
3 Results and Discussion	8
3.1 Satellite data coverage	8
3.2 SST and CHLA seasonal cycles and climatology	13
3.2.1 Satellite versus <i>in situ</i> sea temperature	13
3.2.2 Quality Control of Buoy Data: the North Hecate case	15
3.2.3 Gwaii Haanas Temperature in Relation to Bonilla Island Light station	18
3.2.4 Climatology and seasonal cycle at the synoptic scale	20
3.3 Environmental indices	21
3.3.1 Time series and trend analysis	21
3.3.2 Number of days with SST ≥ 11 in Gwaii Haanas	27
3.3.3 Marine heatwave in 2018-2019	29
3.3.4 Cumulative CHLA	31
4 Conclusion	33
Acknowledgement	34
A Monthly bias for light station and buoy sites	37
B SST climatology and anomaly for 2018-2019	42

List of Tables

1	Boundary coordinates for the subregions of interest.	3
2	Coordinates of light stations where daily <i>in situ</i> water temperature were recorded .	3
3	Coordinates of buoys where daily <i>in situ</i> water temperature was recorded	4
4	Day of year (doy) and seasonal assignment for each month	8
5	Linear regression of satellite data versus <i>in situ</i> measurements for the three buoys	14
6	Linear regression of satellite data versus <i>in situ</i> measurements for the three light-stations	15
7	The MAE, MAPE, MRE, and MRPE for buoys	17
8	The MAE, MAPE, MRE, and MRPE for light stations	17
9	Linear regression of Bonilla Island versus Gwaii Haanas satellite SST data for the three regions	19
10	Summary of slope, standard error, and p-value for the seasonal linear regression . .	22
11	Consecutive days where SST was above or below 11 deg in Gwaii Haanas	29
12	The mean, minimum, and maximum cumulative total in each region.	31
13	The first day where cumulative CHLA reaches the threshold.	32
A.1	Monthly bias Amphitrite Point	38
A.2	Monthly bias Bonilla Island	38
A.3	Monthly bias Langara Island	39
A.4	Monthly bias Middle Nomad	39
A.5	Monthly bias North Hecate	40
A.6	Monthly bias La Perouse	40

List of Figures

1	Bathymetry of the area that contains all of the regions	2
2	Spatial percent coverage (%) of SST and CHLA for the region	9
3	Temporal coverage (%) of SST data	11
4	Temporal coverage (%) of CHLA data	12
5	Percent of available SST data for each month in each region	13
6	Satellite SST versus <i>in situ</i> SST for the three lightstations and three buoys	16
7	Daily SST timeseries for North Hecate in 2018-2019	18
8	Satellite versus <i>in situ</i> SST North Hecate weather buoy for 2018-2019	18
9	Correlation plot of the daily mean satellite-derived SST for all Gwaii Haanas regions versus Bonilla Island at various spatial resolutions	20
10	Weekly climatology of SST and CHLA	21
11	Monthly mean SST time series of AOI, SK-B, and SI	23
12	Monthly mean SST time series for Gwaii Haanas	24
13	AOI, SK-B, and SI monthly time series for CHLA	26
14	Gwaii Haanas regions monthly time series for CHLA	27
15	Interpolated daily SST data for the Gwaii Haanas area	28
16	The total number of days where the mean SST was $\geq 11^{\circ}\text{C}$ for Gwaii Haanas	28
17	Comparison of coverage for the different SST composites in 2018	30
18	October-2018 SST anomaly	31
19	Cumulative CHLA based on interpolated CHLA daily geometric mean	33
B.1	Monthly climatology for SST from 1990 to 2003	42
B.2	Monthly composite for SST in 2018	43
B.3	Monthly composite for SST in 2019	44
B.4	Monthly comparison for SST in 2018	45
B.5	Monthly comparison for SST in 2019	46

ABSTRACT

Devred, E., Hardy, M., and Hannah, C. 2021. Satellite observations of the Northeast Pacific Ocean. Can. Tech. Rep. Hydrogr. Ocean Sci. 335: vii + 46 p.

Satellite ocean colour and thermal imaging provide unique information on the biogeochemical properties of the ocean, which are routinely included in the reporting of the Monitoring Program for the Atlantic Zone and Atlantic Zone Off-shelf. This report lays the ground for routine processing of satellite-derived chlorophyll-a concentration (CHLA) and sea-surface temperature (SST), as well as the development of a set of metrics that will inform on the state of the Pacific Ocean, notably the Northeast Pacific and in six areas of interest: SGaan Kinghlas-Bowie Seamount MPA, Scott Islands Marine National Wildlife Area, Pacific Offshore Area of Interest, and the Gwaii Haanas National Parks Reserve/National Marine Conservation Area Reserve/Haida Heritage Site. A 38-year time series of SST (1981-2018) from the Advanced Very High Resolution Radiometer (AVHRR) sensor and a 16-year time series of CHLA (2003-2018) from the moderate resolution imaging spectroradiometer (MODIS-Aqua) were used to infer seasonal cycle, trends, and cumulative chlorophyll-a concentration, in the areas of interest. In addition, information on satellite spatio-temporal coverage was provided to help interpret the data. Comparison of SST with *in situ* data from moorings and weather stations was carried out to detect possible bias in the data. This comparison revealed a shift in temperature due to instrumentation failure at a buoy located in North Hecate in 2018 and 2019. Trend analysis revealed an increase in SST in winter in all regions and in winter, summer, and fall in Scott Islands Marine National Wildlife Area. We also investigated whether cumulative chlorophyll-a concentration could be a good indicator of the trophic state of the study areas. This set of satellite-based tools allows the update of the satellite time series and the retrieval of ecosystem metrics in a systematic and efficient manner.

RÉSUMÉ

Devred, E., Hardy, M., and Hannah, C. 2021. Satellite observations of the Northeast Pacific Ocean. Can. Tech. Rep. Hydrogr. Ocean Sci. 335: vii + 46 p.

L'imagerie satellitaire de la couleur des océans et du signal thermique fournit une information unique sur les propriétés biogéochimique de l'océan, qui est inclus régulièrement dans les rapports du programme de monitoring de la Zone Atlantique et de la Zone Hauturière Atlantique. Ce rapport pose les bases du traitement de routine de la concentration en chlorophylle-a (CHLA) et de la température de surface de la mer (SST) dérivée des satellites, ainsi que du développement d'un ensemble de paramètres qui informeront sur l'état de l'océan Pacifique, notamment le Pacifique Nord-Est et dans sept zones d'intérêt: la ZPM SGaan Kinghlas-Bowie Seamount, la réserve marine nationale de faune de l'île Scott, la ZPM Endeavour Hydrothermal Vents, la zone d'intérêt au large du Pacifique et la réserve de parcs nationaux / réserve d'aires marines nationales de conservation combinées de Gwaii Haanas / Site du patrimoine haïda. Une série chronologique de 38 ans de SST (1981-2018) du capteur radiomètre avancé à très haute résolution (AVHRR) et une série chronologique de 16 ans de CHLA (2003-2018) du spectroradiomètre d'imagerie à résolution modérée (MODIS-Aqua) ont été utilisées pour déduire le cycle saisonnier, les tendances, la concentration cumulative de chlorophylle-a dans les zones d'intérêt. En outre, des informations sur la couverture spatio-temporelle des satellites ont été fournies pour aider à interpréter les données. Une comparaison de la SST avec les données in-situ de mouillages instrumentés et des stations météorologiques a été réalisée pour détecter d'éventuels biais dans les données. Cette comparaison a révélé un changement de température dû à une défaillance de l'instrumentation à une bouée située à Norths Hecate en 2018 et 2019. L'analyse des tendances a révélé une augmentation de la SST en hiver dans toutes les régions et en hiver, été et automne dans la réserve nationale de faune marine de l'île Scott. Nous avons également étudié si la concentration cumulative de chlorophylle-a pouvait être un bon indicateur de l'état trophique des zones d'étude. Cet ensemble d'outils satellitaires permet la mise à jour des séries chronologiques satellitaires et la récupération des mesures écosystémiques de manière systématique et efficace.

1 Introduction

Satellite remote sensing provides an efficient way to observe oceans at a synoptic scale with high revisiting frequency. In particular, satellite ocean colour informs on the biological activity (primary producers) of the upper layer of the ocean (tens of meters). By inverting the visible signal that leaves the seawater, it is possible to retrieve the concentration of chlorophyll-a pigment (CHLA in mg m^{-3}), an index of phytoplankton biomass. By aggregating this information over time and space, it becomes possible to derive information on phytoplankton phenology and assess the status of the marine ecosystems. In addition to visible radiation, satellites also measure the thermal signature of the very superficial temperature of the ocean, referred to as sea-surface temperature (SST in $^{\circ}\text{C}$). Together, SST and CHLA provide an assessment of the status of the marine ecosystem and the use of long-term time series (e.g., several decades) allows detection and quantification of changes and trends. In the DFO Maritimes and Quebec regions, satellite remote sensing of SST and CHLA has been used for a decade or so to report on the health of the Atlantic Ocean (DFO, 2018, 2019). For instance, time series of chlorophyll-a concentration are summarized in environmental indices, in particular, the spring bloom is characterized by its initiation time, duration, and magnitude. Semi-monthly composites of SST anomalies are also produced to identify zones of unusual warming and cooling.

For the Northeast Pacific, satellite remote sensing of ocean color has remained a marginal product to inform on the state of the Pacific Ocean and it has mainly been used in a topical manner (Perry, 2014; Chandler et al., 2017) rather than in a systematic approach with consistent products reported on an annual basis. This current report discusses the use of satellite ocean colour and sea-surface temperature to quantify baseline conditions and changes in the Northeast Pacific along with seven areas of interest; SGaan Kinghlas-Bowie Seamount MPA (thereafter referred to as Bowie Seamount MPA for simplicity), Scott Islands Marine National Wildlife Area, Endeavour Hydrothermal Vents MPA, Pacific Offshore Area of Interest, and the Gwaii Haanas National Parks Reserve/National Marine Conservation Area Reserve/Haida Heritage Site (thereafter referred to as Gwaii Haanas, which is further divided into 3 areas for the purpose of our study). We used the Advanced Very High Resolution Radiometer (AVHRR) and the MODerate resolution Imaging Spectrometer on the Aqua platform (MODIS-Aqua) to retrieve sea-surface temperature and chlorophyll-a concentration, respectively. The current report objectives are not only to derive baseline conditions, but also to report on trends over the last few decades, and to propose ecosystem indices. It also lays the groundwork for a routine monitoring of the Northeast Pacific that could be included in DFO's annual reporting. We acknowledge that improvements to the products presented in this report will be carried out in the coming years, and new products might be required following the publication of this technical report. Note that the Strait of Georgia and Salish Sea were not included in the study as the spatial resolution of the satellite archive (i.e., 4 km) was too coarse for these regions, in addition, given the optical complexity of this environment (i.e., co-occurrence of dissolved material, mineral particles, and phytoplankton), specific algorithms need to be developed and validated for these areas (Carswell et al., 2017).

2 Data and Methods

2.1 Region of Interest

The present study focuses on the Northeast Pacific Ocean within an area bounded by 124 to 140 °W and 44 to 55 °N. Within this area, satellite data were extracted for seven regions of interest, given their status of Ecologically and Biologically Significant Areas (EBSAs) or classification as Marine Protected Areas (MPAs), these regions include Bowie Seamount MPA (SK-B), Gwaii Haanas (divided into three areas: west (GHW), east (GHE) and south (GHS)), Scott Islands NWA (SI), Offshore Pacific Area of Interest (AOI), and Endeavour Hydrothermal Vents MPA (EHV). See Figure 1 for the bathymetry of the region with the seven regions of interest. These regions vary in size, with the largest being AOI spreading over thousands of square kilometers to the smallest EHV region that consists only of three to four 4km-resolution pixels (Table 1).

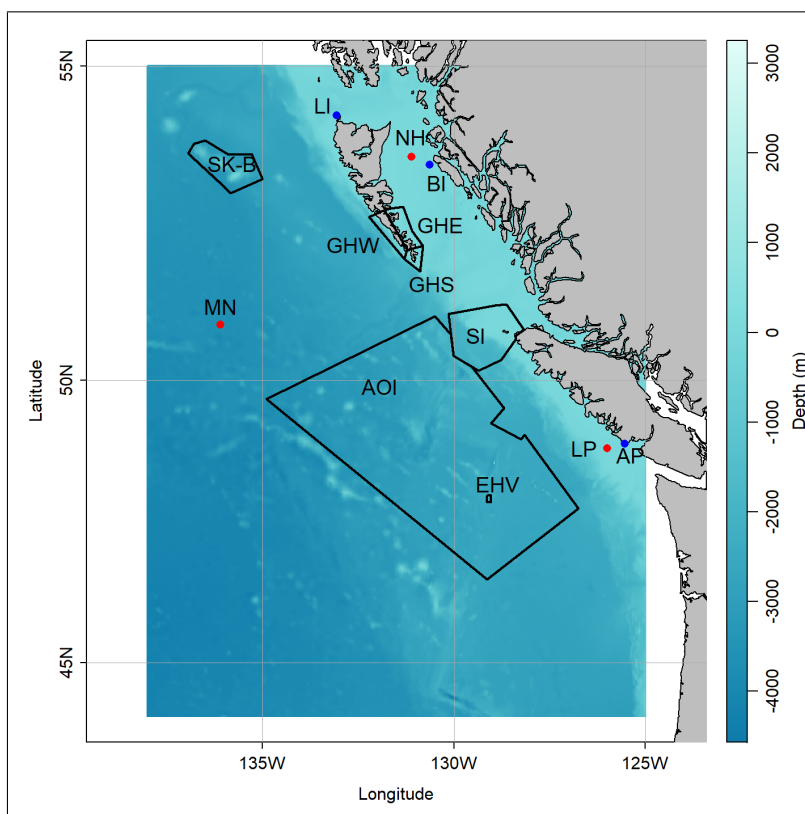


Figure 1: Bathymetry of the area that contains the seven regions in the west coast (black line boundaries), the three lightstations (blue points), and the three buoys (red points). Bowie Seamount MPA (SK-B), Gwaii Haanas west (GHW), Gwaii Haanas east (GHE), Gwaii Haanas south (GHS), Scott Islands NWA (SI), Offshore Pacific Area of Interest (AOI), Endeavour Hydrothermal Vents MPA (EHV), Langara Island (LI), Bonilla Island (BI), Amphitrite Point (AP), La Perouse (LP), Middle Nomad (MN), and North Hecate (NH).

2.2 Data

2.2.1 *In situ* Temperature

In addition to the seven regions of interest for satellite data extraction, *in situ* measurements from the British Columbia Shore Station Oceanographic Program (BCSOP) were used for comparison

Table 1: Boundary coordinates for the subregions of interest. For the individual Gwaii Haanas (GH) subregions, points are: West boundary (5 → 6 → 7 → 9), East boundary (9 → 1 → 2 → 3 → 4), and South boundary (1 → 8 → 7 → 9). All boundaries are closed at their respective first point.

* Point 9 under GH isn't included in the large Gwaii Haanas box, it is only for separating the three smaller subregions (GHW, GHE, and GHS).

Point	AOI		SK-B		EHV		GH*		SI	
	Lat (°N)	Lon (°W)								
1	49.68	-134.90	53.05	-135.84	47.90	-129.03	52.21	-130.82	50.69	-128.38
2	51.06	-130.51	53.27	-135.00	47.90	-129.13	52.45	-131.09	50.35	-128.76
3	50.77	-130.08	53.66	-135.28	48.02	-129.13	52.83	-131.34	50.16	-129.35
4	50.41	-130.01	53.66	-135.90	48.02	-129.03	52.81	-131.66	50.41	-130.01
5	50.23	-129.53	53.87	-136.51			52.78	-131.82	51.10	-130.14
6	49.53	-128.69	53.82	-136.79			52.68	-132.22	51.24	-128.93
7	49.27	-129.03	53.67	-136.95			52.00	-131.30	51.25	-128.78
8	49.00	-128.25	53.23	-136.17			51.80	-130.89	51.25	-128.61
9	49.07	-128.16					52.15	-131.23	50.84	-128.18
10	47.79	-126.75							50.74	-128.40
11	46.53	-129.13							50.73	-128.39

with sea-surface temperature measured by satellite. BCSOP presently monitors sea-surface temperature and salinity at 12 stations located along the British Columbia shore. *In situ* data are gathered from a bucket of water collected at the surface at, or near, daytime high tide. For our studies only three stations were selected: Bonilla Island, Langara Island, and Amphitrite Point (see table 2 for coordinates). Langara Island and Bonilla Island were selected because of their proximity to the Gwaii Haanas region, which is of specific interest. Amphitrite Point was selected because of its proximity to three regions of interest (AOI, EHV, and SI). Because temperature is measured around high tide during the day, a delay of about 50 min is introduced from day to day. A cycle of 14 days is necessary to sample the temperature at the same time of the day, therefore there is a temperature daily cycle that is introduced in the measurements. However, this daily cycle is reduced when the monthly means are computed. The difference in temporal and spatial scales (4-km resolution SST against a few liters of water collected using a bucket from shore and daily variation in time of data collection) inherently introduces uncertainties in the comparison between the satellite and *in situ* measurements, which has to be kept in consideration while performing the analysis. The data collected from Bonilla Island, Langara Island, and Amphitrite Point span from 25/08/1981 to 30/11/2019. Light station data were retrieved from Fisheries and Oceans Canada website (<http://www.pac.dfo-mpo.gc.ca/science/oceans/data-donnees/lightstations-phares/index-eng.html>).

Table 2: Coordinates of light stations where daily *in situ* water temperature were recorded.

Light Station	Latitude (°N)	Longitude (°W)
Bonilla Island (BI)	53.4928	-130.6358
Langara Island (LI)	54.2564	-133.0583
Amphitrite Point (AP)	48.9222	-125.5408

In situ temperature (at sea level; 0 m) from weather buoys were also used for comparison with satellite SST. These weather buoys are monitored and maintained by Environment and Climate Change Canada (ECCC) as part of their national network. There is currently a total of sixteen offshore weather buoys on the west coast of Canada, for this study we have chosen three weather buoys: La Perouse Bank (station 46206), Middle Nomad (station 46004), and North Hecate Strait (station 46183) (see table 3 for coordinates). The data from La Perouse Bank buoy spans from 22/11/1988 to 31/12/2019; Middle Nomad spans from 04/08/1988 to 31/12/2019; North Hecate span from 15/05/1991 to 15/10/2019 (note that dates for which no satellite data were available were excluded from our study). More information on the weather buoys can be found on the National Data Buoy Center website(<https://www.ndbc.noaa.gov/>).

Table 3: Coordinates of buoys where daily *in situ* water temperature was recorded.

Buoy	Latitude (°N)	Longitude (°W)
La Perouse (LP)	48.84	-126.00
Middle Nomad (MN)	50.93	-136.10
North Hecate (NH)	53.62	-131.10

2.2.2 Satellite Data

2.2.2.1 Sea-Surface Temperature

Global daily sea-surface temperature (SST) consisted of the Pathfinder version 5.3 daily Advanced Very High Resolution Radiometer (AVHRR) time series with a nominal resolution of 4-km at the equator. The data were downloaded from the National Oceanic and Atmospheric Administration website (NOAA, https://data.nodc.noaa.gov/cgi-bin/iso?id=gov.noaa.nodc:AVHRR_Pathfinder-NCEI-L3C-v5.3) and stored in netCDF format on a server at the Bedford Institute of Oceanography (BIO). The data used in this study spans from 25/08/1981 to 31/12/2019. The global dataset was subset to the region of interest and also stored in netCDF format to reduce the storage requirements and speed up processing time. Quality flags associated with the SST data range from one to five, with five being the highest quality. In the current analysis, we retained only SST data with a quality flag greater than or equal to four to ensure that only the most reliable data were used.

2.2.2.2 Chlorophyll-a concentration

Global daily chlorophyll-a concentration (CHLA) images at 4-km resolution from the MODerate resolution Imaging Spectroradiometer (MODIS) on the Aqua platform were downloaded from the National Aeronautic and Space Administration website (<https://oceancolor.gsfc.nasa.gov>). The data spans from 01/01/2003 to 31/12/2019, corresponding to 17 years of observations. The global images were subset to a pan-Canadian grid that includes Canada’s three oceans and data for the region of interest were further extracted. The chlorophyll-a product is based on the standard OC3M algorithm from NASA, a detailed description can be found on their website (https://oceancolor.gsfc.nasa.gov/atbd/chlor_a/). Briefly, ratios of remote sensing reflectance (R_{rs}) at several wavebands are related to chlorophyll-a concentration to account for the change in water

colour as chlorophyll-a concentration increases using a fourth degree polynomial function, which coefficients were determined using an extensive database of *in situ* measurements.

2.3 Methods

All data handling and computational aspects of this project were coded in R language (<http://cran.r-project.org/>) and are available on a Github repository. Access to the repository is available on demand.

2.3.1 Daily and Monthly Mean

For a given region, the mean daily SST was derived by computing the arithmetic average of all valid pixels on that day in that region, the percentage proportion of the number of valid pixels along with the total number of pixels in a region was saved for quality control and statistical purposes. The monthly composite of SST was also computed using arithmetic average of all data available for a given region in that month.

The daily geometric mean of CHLA concentration was computed for each region for the entire time series and the percentage of valid pixels to total number of possible pixels were saved for quality control and statistical purposes. The data were further binned into a monthly time series using the geometric average of all data available within a region and month. Aside, assessment of satellite-derived CHLA concentration against CHLA concentration measured *in situ* using high performance liquid chromatography (HPLC) revealed a small bias when linearly regressing satellite against *in situ* data (slope of 0.97 and intercept of 0.021, $r^2=0.59$) and a root-mean square log error (RMSLE) of 0.37, details on the performance of CHLA algorithms in the Northeast Pacific can be found in (Clay et al., 2019).

2.3.2 Temporal and Spatial Cover

Daily temporal coverage (%) for a given region was computed in a similar fashion for both SST and CHLA by summing the number of valid pixels in each year for a given day of year (doy), then dividing it by the total number of pixels in the region (area of region \times number of years) and multiplying by 100%. For instance, if there is a total number of 804 available pixels of CHLA data over 17 years of observation for day of year 235 in an area containing 150 pixels, the temporal percentage coverage for that day will be expressed as $\frac{804}{150 \times 17} \times 100\% = 32\%$. This step was repeated for each day of year to obtain the temporal coverage (%) for each region.

Daily spatial coverage (%) was computed in a similar manner as the percent temporal coverage but for the entire area containing all regions of interest (bounded by 124 to 140 °N and 44 to 55 °W). For each individual pixel within the area, the total number of available valid pixels was summed and divided by the total number of days. For instance, if a given pixel had valid data for 3203 days out of the 17 years (for a possible total of $17 \times 365 + 4 = 6205$ days), then the spatial coverage for that individual pixel equals $\frac{3203}{6205} \times 100 = 52\%$. This was repeated for each pixel within the Northeast Pacific and plotted on a map to show the spatial coverage (%).

2.3.3 Seven-day Climatology

The seven-day climatology was computed for both CHLA and SST for all regions and surrounding area. This time scale was selected to resolve short term variation that is not captured by monthly

data while reducing the number of missing data associated with low temporal resolution (i.e., 1 to 3 days). The weekly climatology was calculated by taking the average of all the data available in a given week across all years (total of 52 weeks). The weekly composites were further binned into seasonal composites to emphasize the seasonal cycle, in particular for SST. The weeks were seasonally binned as follows: winter includes weeks 1 to 13, spring includes week 14 to 26, summer includes weeks 27 to 39, and fall includes weeks 40 to 52.

2.3.4 Environmental indices

While providing values of SST and CHLA at large spatial scales informs on the overall status of the marine ecosystem, there is a need to synthesis the information in a more meaningful way that can be directly used by non-experts, managers, and decision-makers. In consultation with local experts, it was decided to test four environmental metrics that are relevant to the functioning of the marine ecosystem and provide a rapid assessment of its status. These metrics are SST anomalies, comparing satellite-derived SST with *in situ* measurements, number of consecutive days of SST higher than 11°C, cumulative CHLA concentration, and the linear trends of any time series of SST and CHLA in all the regions of interest.

2.3.4.1 SST Anomalies

SST anomalies were computed to reveal abnormal patterns in SST dynamics and in particular marine heatwaves that have been observed in the Northeast Pacific ocean over the last few years, notably during the 2013-2015 and 2018-2019 periods. Composite images were computed using three different time spans of 8-day, 14-day, and one month to determine the optimal spatial coverage that captures peaks in SST. Monthly composites were retained for the spatio-temporal analysis of the warm waters spreading along the Pacific coast as they provide images with the least data gaps while resolving spatial temperature gradients.

The monthly SST composites were calculated by taking the mean of all SST data available at each pixel for each month in the year of interest. Each pixel-based individual monthly mean was saved into a netCDF file and png files were generated for visual analysis. The reference monthly climatology was calculated using the period 1990 to 2003; this was done in a similar process to the monthly SST composites. Anomalies were derived by subtracting the monthly climatology (1990-2003) from the monthly composite data.

2.3.4.2 Satellite versus *in-situ* SST data

For the light station and buoy sites, the daily *in situ* SST data were compared to the Pathfinder AVHRR satellite-derived SST data. We tested the effect of the number of pixels used to extract the daily satellite SST data with *in situ* SST data to find the best compromise between spatial averaging and number of data available. Satellite SST was therefore extracted for six different box sizes, all centered on the buoy site and corresponding to 1, 9 (3x3), 25 (5x5), 36 (6x6), and 64 (8x8) pixels. A Model II linear regression model was applied on the satellite SST against the *in-situ* SST, type II regression is applied when both the x and y variables are assumed to contain uncertainties, see section 10.3.2 of Legendre and Legendre (2012), while the commonly used (i.e., model-I) linear regression assumes that the x variable is free of uncertainties. In addition to the slope and intercept

of the linear regression as a metric for performance, the mean absolute error (MAE), mean absolute percent error (MAPE), mean relative error (MRE), and mean relative percent error (MRPE) were also calculated to inform on the uncertainties associated with satellite SST (Equations 1, 3, 2, and 4).

$$MAE = \sum_{i=1}^{i=N} |(SST_{sat} - SST_{is})| \quad (1)$$

$$MAPE = \sum_{i=1}^{i=N} \frac{|(SST_{sat} - SST_{is})|}{SST_{is}} \times 100 \quad (2)$$

$$MRE = \sum_{i=1}^{i=N} (SST_{sat} - SST_{is}) \quad (3)$$

$$MRPE = \sum_{i=1}^{i=N} \frac{(SST_{sat} - SST_{is})}{SST_{is}} \times 100 \quad (4)$$

A similar approach was also applied to the satellite-derived SST data for the three Gwaii Haanas regions versus the Bonilla Island light station. The daily SST data obtained from the various sizes (1 to 64 pixels) at Bonilla Island were tested to see if it would have an impact when plotted against the three Gwaii Haanas regions (east, west, and south) satellite-derived SST data. The objective of this effort is to find a relationship between the lighthouse and the satellite SST at Gwaii Haanas to extend the temperature record at Gwaii Haanas to the length of the lighthouse time series (i.e., back to 1961)

2.3.4.3 SST number of days above 11°C

The number of consecutive days where the SST was ≥ 11 °C for a given year was determined for the Gwaii Haanas area using interpolated data. The daily mean SST was filtered to only include data with a spatial percent coverage $\geq 10\%$. Linear interpolation was chosen to fill missing data to obtain a time series of continuous data to count the number of days when SST was greater than 11°C. In some years (e.g., 1983, 1996 and 2006), SST remained over 11°C continuously resulting in a single value for the number of days over 11°C while for other years (e.g., 2000 and 2016), SST oscillated around the values of 11°C such that several periods when the criteria was met were recorded. In that case, the total number of days with SST greater than 11°C was also recorded.

2.3.4.4 Cumulative chlorophyll-a concentration

Phytoplankton bloom initiation, magnitude, and duration is not characterized as well in the North-east Pacific as in the Northwest Atlantic (Cole et al., 2015), such that inferring bloom metrics with generic methods such as the shifted Gaussian is challenging. Here, we tested the possibility to use cumulative chlorophyll-a concentration to obtain a measurement of the health of the marine ecosystem and in particular the ability of primary producers to sustain higher trophic levels.

The daily geometric mean CHLA was filtered to remove daily means with less than 10% of spatial coverage; this criterion was chosen to ensure that daily means with a small amount of data would not weigh on any annual time series. As for SST, missing data within any annual time series were filled using linear interpolation (*approx()* function in R). The cumulative CHLA was computed from the interpolated data for each year and each region by summing daily mean chlorophyll-a concentrations.

2.3.4.5 Time series analysis

To monitor changes and derive rates of change, linear regression of properties (e.g., monthly CHLA and SST) against time was performed for all regions. Only results at the 0.05 significance level (i.e., p-value lower than 0.05) were recorded and reported in this document.

Table 4: Day of year (doy) and seasonal assignment for each month.

	Winter			Spring			Summer			Fall		
	Jan	Feb	Mar	Apr	May	Jun	Jul	Aug	Sep	Oct	Nov	Dec
Start	1	32	60	91	121	152	182	213	244	274	305	335
End	31	59	90	120	151	181	212	243	273	304	334	366

The monthly mean SST for Gwaii Haanas regions (east, west, and south) were plotted, individually, against the monthly SST data from the light stations (Bonilla and Langara). A linear model function was applied to each pair of data sets (a total of 6). The linear equation (slope and intercept), R^2 , and the adjusted R^2 were extracted from the linear model summary output.

2.3.4.6 Satellite vs. *in situ* at the monthly scale

Performance of the satellite-derived SST was assessed against each *in situ* site (light stations and weather buoys) to detect potential biases. Five different surface areas represented by a given number of pixels were used to extract the satellite-derived SST: 1 pixel, 9 pixels, 25 pixels, 36 pixels, and 64 pixels. For each month over the span of 41 years, a linear regression model was applied on the satellite-derived SST against the *in situ* SST ($\text{lm}(\text{satelliteSST} \sim \text{insituSST})$). There were 4 variables of interest, the intercept, the slope, r^2 , and N (the number of days with available data). For the North Hecate weather buoy, it was noted there was a drift beginning in the middle of 2018 and carried to 2019. The statistics provided for the North Hecate site do not include 2018 and 2019 due to this drift in temperature measurements.

3 Results and Discussion

3.1 Satellite data coverage

While ocean colour and thermal imageries are powerful tools to monitor the marine ecosystem, one of the main drawbacks of these earth observation tools is their inability to collect data under cloud cover. In that respect, the Northeast Pacific is a challenging area given the low daily coverage of the region, which has to be taken into account when analyzing the data. A common method to circumvent the issue of data gap is to spatially and temporally bin the data. It is also important to note that the size of the seven regions of interest vary greatly. The EHV region is the smallest and

consisted of only a few 4 km-resolution pixels and while we have carried out analysis for this small region, higher resolution (250 to 300 m resolution) would be better adapted to obtain meaningful results. The Gwaii Haanas regions also consisted of a few pixels, which are located close to the coast. We recommend the use of high-resolution imagery for this region to ensure higher quality results. On the other end, the AOI is the largest region and spans over thousands of square kilometers (approximately 137,058 km²), which allows the current resolution to be appropriate for studying this area.

In general, the pixel-based spatial coverage (%) of SST is low and varies between 1 and 20% for the Northeast Pacific while the results for pixel-based spatial coverage (%) of CHLA are slightly higher with values up to 25%. The nearshore areas exhibit a low percent coverage for both SST and CHLA ($\leq 2\%$), perhaps due to local effects such as fog. The spatial coverage increases offshore and reaches values of about 18% and 25% for SST and CHLA, respectively. In the pelagic environment the temporal coverage decreases again and varies between 1% and 10%. Some of the Northeast Pacific is seldom observed by satellites. See figure 2 for the mapped spatial coverage (%) for SST and CHLA for all regions and their surroundings.

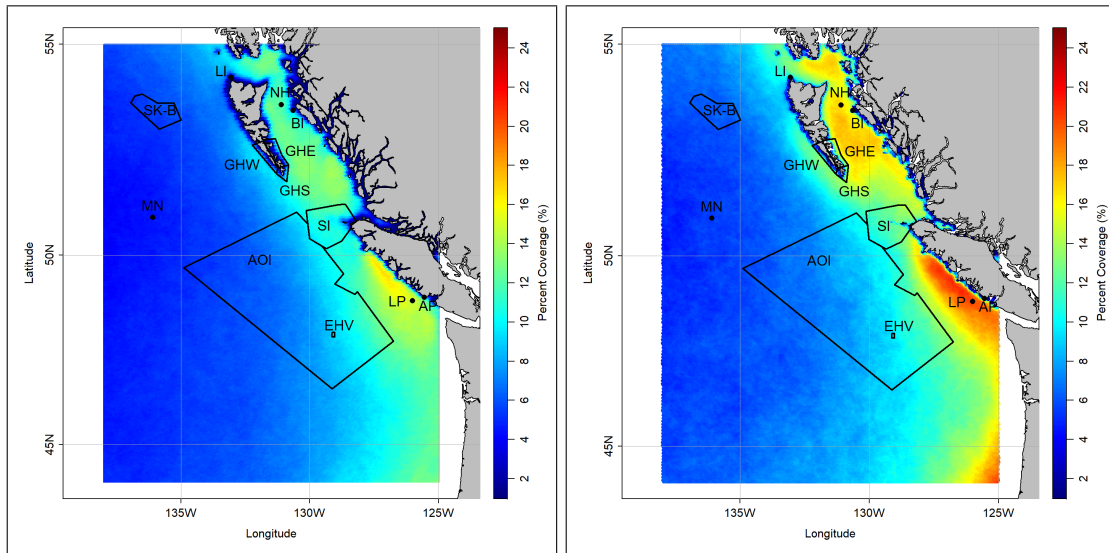


Figure 2: Spatial percent coverage (%) of SST (25/08/1981 to 31/12/2019) and CHLA (01/01/2003 to 31/12/2019) for the region.

The temporal coverage (%) for SST and CHLA follows a bimodal pattern with highest coverage in spring and fall and the lowest coverage in summer and winter. For CHLA in particular, the temporal coverage was very low to non-existent between day of year 310 and 30 (i.e., late fall to early winter) for most regions, which may be due to the low sun zenith angle during the satellite pass that prevents data acquisition, since good data are obtained when sun zenith angle is above 40° (Barnes and Hu, 2016). For both CHLA and SST, the low availability of data in the summer is explained by the increased cloud cover (see Annex A). Given their large size, the AOI and SI regions show the highest overall coverage for SST. For CHLA, the coastal areas (Gwaii Haanas and SI) have the highest overall coverage. See Figures 3 and 4 for the temporal coverage (%) of SST and CHLA for each region, respectively.

The EHV region has the lowest amount of days with available data for SST and CHLA. There were only 11.9% of days containing valid SST data (each day consisting of four 4 km pixels) and 11.6% of days containing valid CHLA data (each day consisting of three 4 km pixels). These values are low compared to other regions which ranged from 20% to 45% and 20% to 65% of days with available data for SST and CHLA, respectively. This lack of data precluded the computation of robust and meaningful statistics. The temporal coverage (%) looks higher for SST and CHLA in the EHV region (Figures 3 and 4), but the small region creates the illusion that there is a large quantity of pixels. In the future, we will investigate the optimal size (i.e., number of pixels) to retrieve meaningful information for the EHV area.

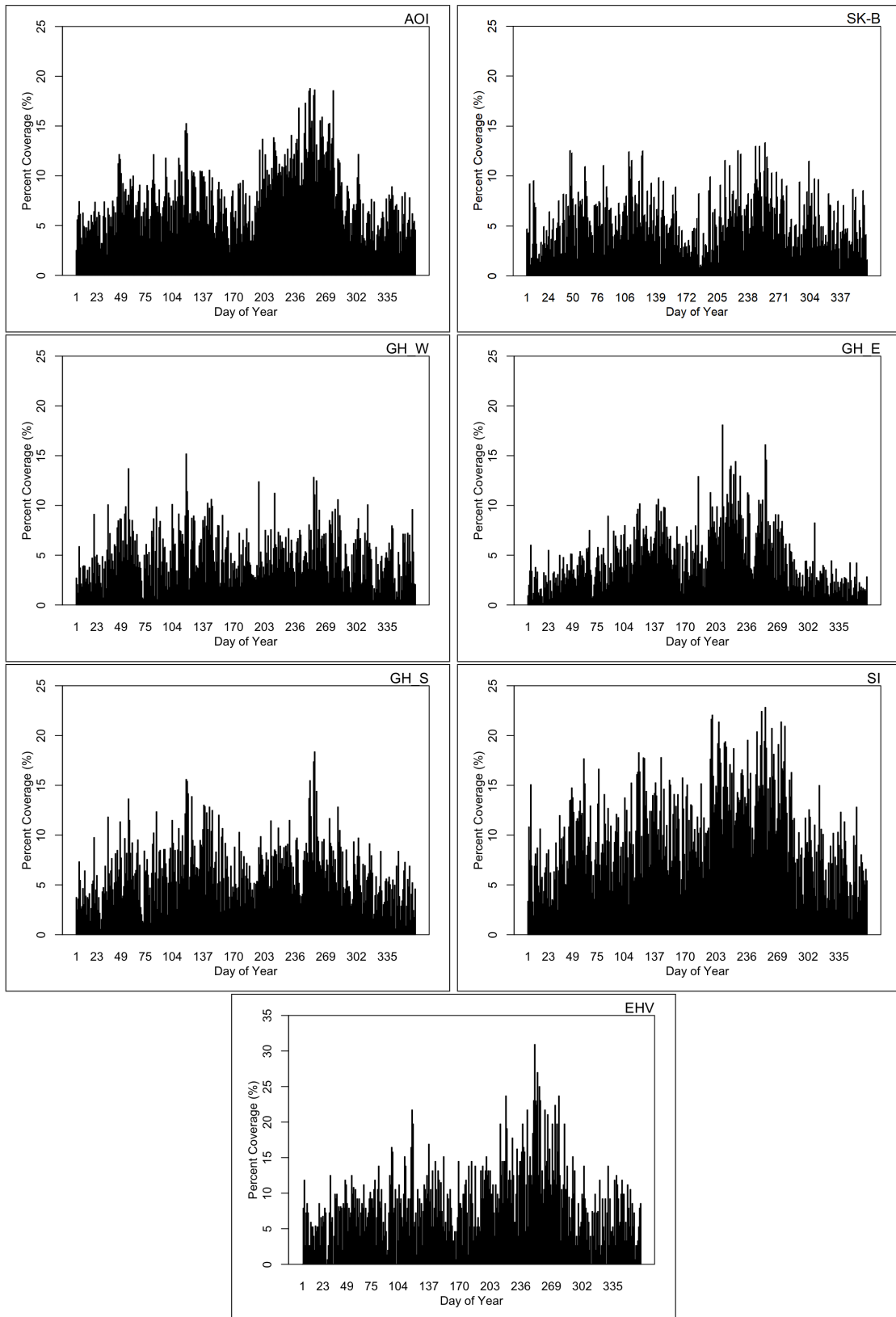


Figure 3: Temporal coverage (%) of SST data from 01/01/1982 to 31/12/2019 for each region. Region labels are in the top right corner. Note the EHV region has a larger range y-axis.

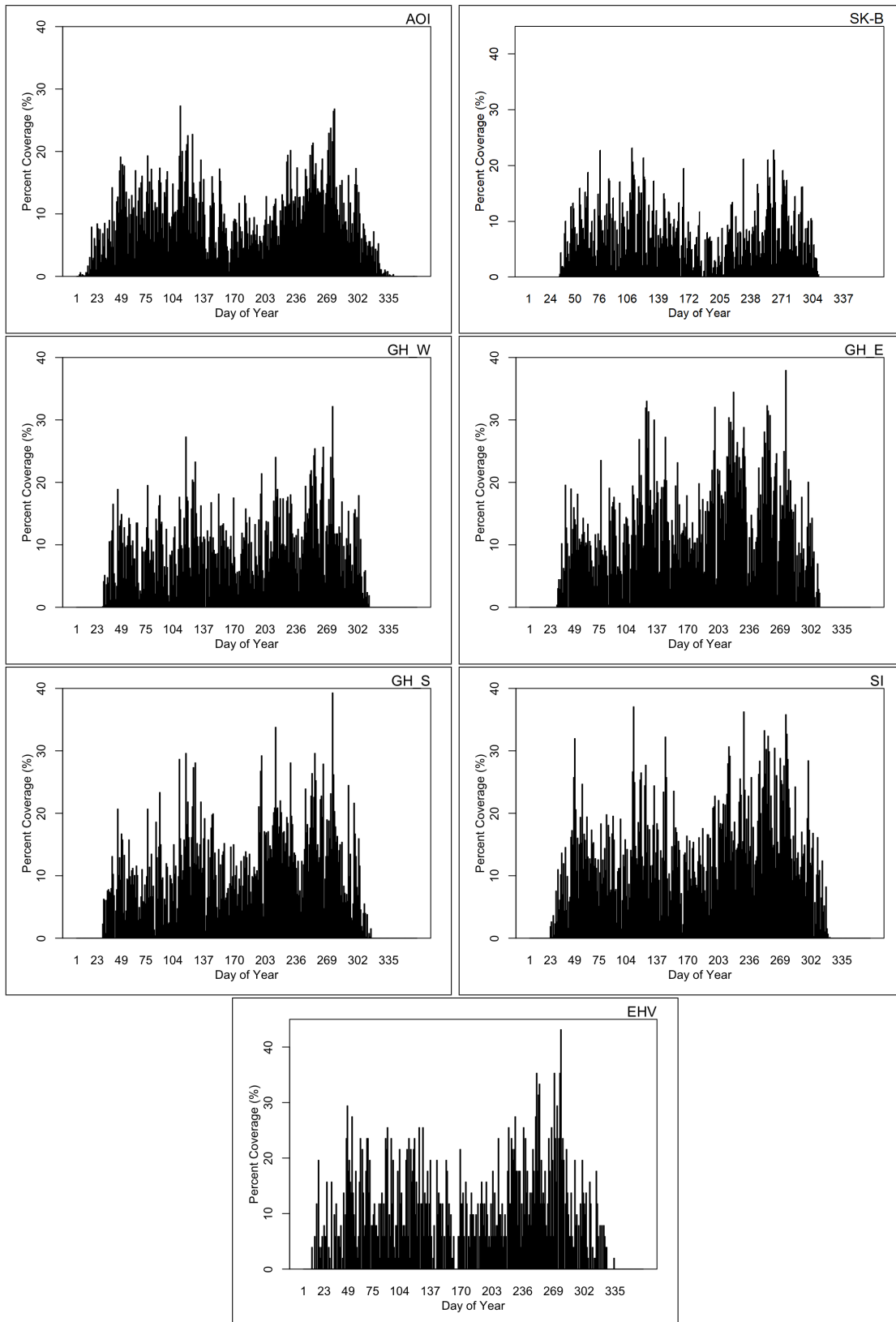


Figure 4: Temporal coverage (%) of CHLA data from 01/01/2003 to 31/12/2019 for each region. Region labels are in the top right corner. Note the EHV region has a larger range y-axis.

The satellite SST data were further binned monthly to demonstrate the lack of available data (Figure 5). Even when the SST data was binned monthly, a majority of months contained less than 10% of data coverage in most regions. Ideally, we would filter out months with less than 10% of data coverage within a region to improve the quality and accuracy of results. But despite this lack of data, all the months were included in the analysis, even those having less than 10% coverage.

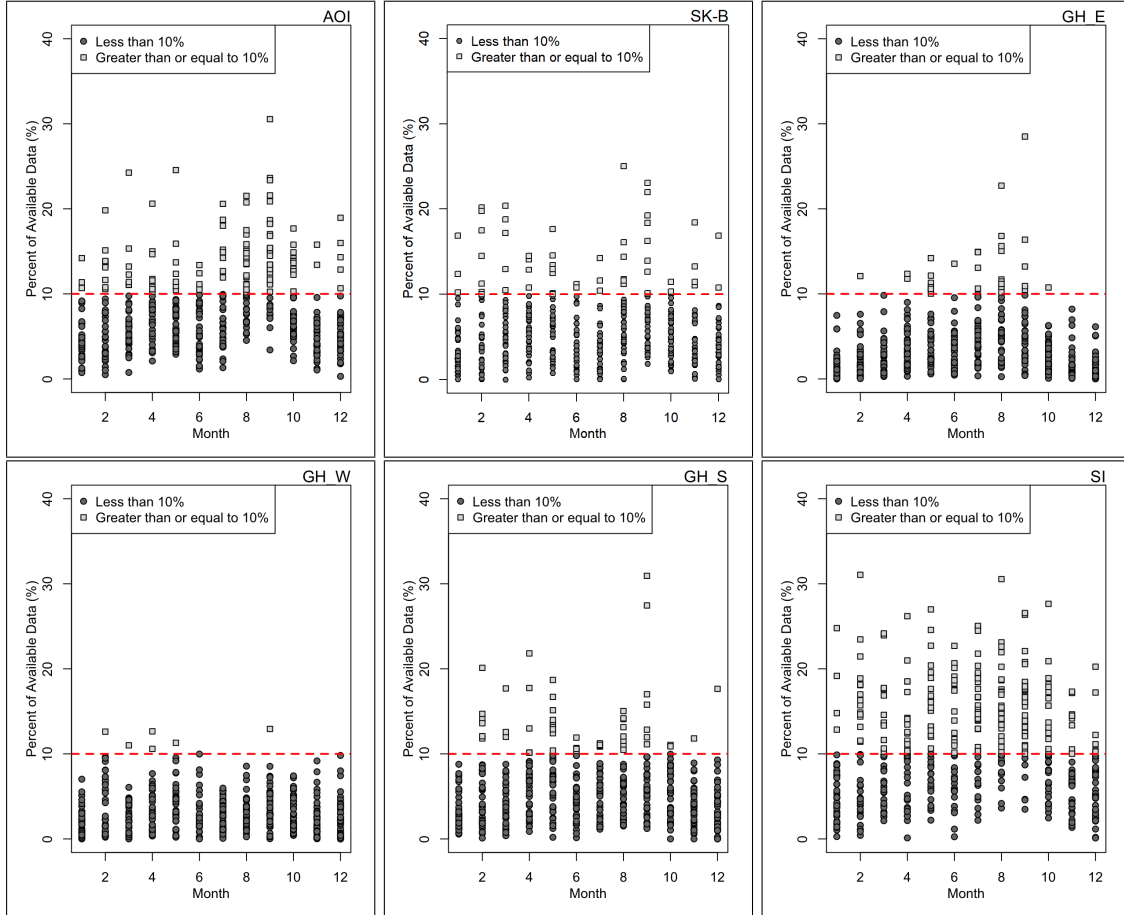


Figure 5: Percent of available SST data for each month in each region from 25/08/1981 to 31/12/2019.

3.2 SST and CHLA seasonal cycles and climatology

3.2.1 Satellite versus *in situ* sea temperature

While satellite-derived SST has a known accuracy of about 0.5°C in the open ocean, far from terrestrial contamination, performance in coastal areas is subject to more variability (Smit et al., 2013; Brewin et al., 2017, 2018). The performance of Pathfinder AVHRR satellite data was tested against *in situ* measurements of temperature on a daily scale for the selected light stations and buoys. The spatial resolution was also tested by expanding the size of the site (1 pixel to 8×8 pixels). For each site (i.e., light station and buoy), the *in situ* daily data were plotted against the satellite-derived daily data (Figure 6).

In general, satellite-derived SST showed a better agreement with the buoy data (e.g., slope ranging between 0.94 ± 0.01 and 0.99 ± 0.01) than with the light station data (slope ranging between 0.83 ± 0.01 and 1.06 ± 0.02). The relationships between satellite and *in situ* measurements are also tighter for the buoy data than for the light station data (Figure 6). As the number of pixels considered to derive SST increases, the number of match ups between satellite and *in situ* data also increases, such that by using 64 rather than a single pixel, the number of match ups are increased by a factor of two to three for the buoy data (e.g., from 1472 to 2993 match ups from one to 64 pixels respectively for the La Perouse buoy) and a factor 3 to 8 for the light station data (e.g., from 325 to 2324 match ups from one to 64 pixels respectively for the Langara Island light station). The slopes of the linear regressions for the buoy data remain fairly constant regardless of the number of pixels used, but the intercepts decrease for the North Hecate and La Perouse buoy with increasing number of pixels used, and we can see the opposite for the Middle Nomad buoy with intercepts increasing with increasing number of pixels. For the buoy data, it seems appropriate to use a bigger area rather than just a single pixel. See Table 5 for the buoy linear regression results.

Table 5: Linear regression of satellite data versus *in situ* measurements for the three buoys: La Perouse (LP), Middle Nomad (MN), and North Hecate (NH). N is the number of match-ups (days where both *in situ* and satellite data are available).

Note: ** p-value < 0.01 and * p-value < 0.1

Site	Pixels	Slope	SE	Intercept	SE	N
LP	One	0.96**	0.01	-0.01	0.08	1472
	3x3	0.96**	0.01	-0.04	0.07	2161
	5x5	0.97**	0.01	-0.1	0.07	2568
	6x6	0.96**	0.01	-0.07	0.07	2717
	8x8	0.96**	0.01	-0.09	0.07	2993
MN	One	0.97**	0.01	-0.2*	0.11	423
	3x3	0.99**	0.01	-0.41**	0.07	787
	5x5	0.98**	0.01	-0.34**	0.06	1084
	6x6	0.98**	0.01	-0.34**	0.06	1237
	8x8	0.97**	0.01	-0.29**	0.06	1440
NH	One	0.95**	0.01	0.1	0.08	1145
	3x3	0.94**	0.01	0.13*	0.07	1692
	5x5	0.94**	0.01	0.13*	0.06	1949
	6x6	0.94**	0.01	0.14*	0.06	2132
	8x8	0.94**	0.01	0.06	0.06	2395

Results of the comparison for the light stations exhibited more variations. For Langara Island light station, the slope remains almost constant and the intercept increases from -0.86 ± 0.23 (at one pixel) to -0.47 ± 0.10 (at 5x5 pixels) but it then decreases again to -0.72 ± 0.08 (at 8x8 pixels) with increased spatial resolution. For Bonilla Island light station, the slope improves, increasing from 0.87 ± 0.01 (at one pixel) to 0.90 ± 0.01 (at 8x8 pixels) and the intercept generally decreases with increasing spatial resolution. Finally for Amphitrite Point light station, the slope decreases from 0.89 ± 0.02 (at one pixel) to 0.83 ± 0.01 (at 8x8 pixels) and the intercept increases from 0.75 ± 0.20 (at one pixel) to 1.53 ± 0.08 (at 8x8 pixels) with increasing spatial resolution. Note that the change of slope and intercept of the linear regression of satellite against *in situ* data for a given site is not a monotonic function of the number of pixels (as discussed with Langara Island (LI) above).

Light stations data may be subject to small scale local effects in addition to the biases induced by sampling time (see section 2.2.1), which explain the difference observed when comparing the satellite data to the *in situ* measurements. The Middle Nomad shows slightly better results than the two other buoys, at least in terms of slope of the regression, which could be explained by the fact that this is the most offshore buoy where the temperature might be the most stable without influences from the coast. See Table 6 for the light station linear regression results.

Table 6: Linear regression of satellite data versus *in situ* measurements for the three lightstations: Amphitrite Point (AP), Bonilla Island (BI), and Langara Island (LI). N is the number of match-ups (days where there is both *in situ* and satellite data available).

Note: ** p-value < 0.01 and * p-value < 0.1

Site	Pixels	Slope	SE	Intercept	SE	N
AP	One	0.89**	0.02	0.75**	0.20	554
	3x3	0.86**	0.01	1.13**	0.11	1918
	5x5	0.85**	0.01	1.24**	0.09	2848
	6x6	0.84**	0.01	1.33**	0.09	3124
	8x8	0.83**	0.01	1.53**	0.08	3550
BI	One	0.87**	0.01	0.72**	0.12	822
	3x3	0.85**	0.01	0.97**	0.09	1611
	5x5	0.86**	0.01	0.87**	0.08	2160
	6x6	0.89**	0.01	0.67**	0.08	2480
	8x8	0.9**	0.01	0.63**	0.07	2832
LI	One	1.06**	0.02	-0.86**	0.23	325
	3x3	1.03**	0.01	-0.52**	0.14	873
	5x5	1.04**	0.01	-0.47**	0.10	1462
	6x6	1.05**	0.01	-0.61**	0.09	1947
	8x8	1.06**	0.01	-0.72**	0.08	2324

The mean absolute error (MAE) is lower for the buoy than for the light stations data with values of 0.51 to 0.64°C for the buoys (Table 7) and values of 0.75 to 0.90°C for the light stations (Table 8). These results are consistent with the expected uncertainties of 0.5°C for satellite-derived SST in the open ocean and higher uncertainties in coastal area subject to small scales hydrodynamic features and influence of tidal cycle. The biases at the light stations were lower than the ones found for a coastal site in southern England, which were around 1.3°C Brewin et al. (2018). The relative errors show a systematic underestimation of SST by AVHRR of about 0.2 to 0.3°C for both the buoys and light stations, which correspond to a relative underestimation of approximately 2 to 4%. The number of pixels used to derive SST (i.e., 1 to 64) has a minimal impact on the relative and absolute differences, it increases roughly around 0.1°C or less with increasing number of pixels. Surprisingly, the biases (i.e., mean relative error) decreases when the number of pixels increases for all the light stations.

3.2.2 Quality Control of Buoy Data: the North Hecate case

Comparison between satellite-derived SST and *in situ* measurements of SST showed good agreement for both buoy and light station data, with small but consistent biases. These results provide confidence that the satellite data can be used for both open ocean and coastal monitoring. In addition, as satellites are consistently evaluated and possible drift corrected, they provide a unique opportunity to monitor the buoy measurements and help detect possible anomalies.

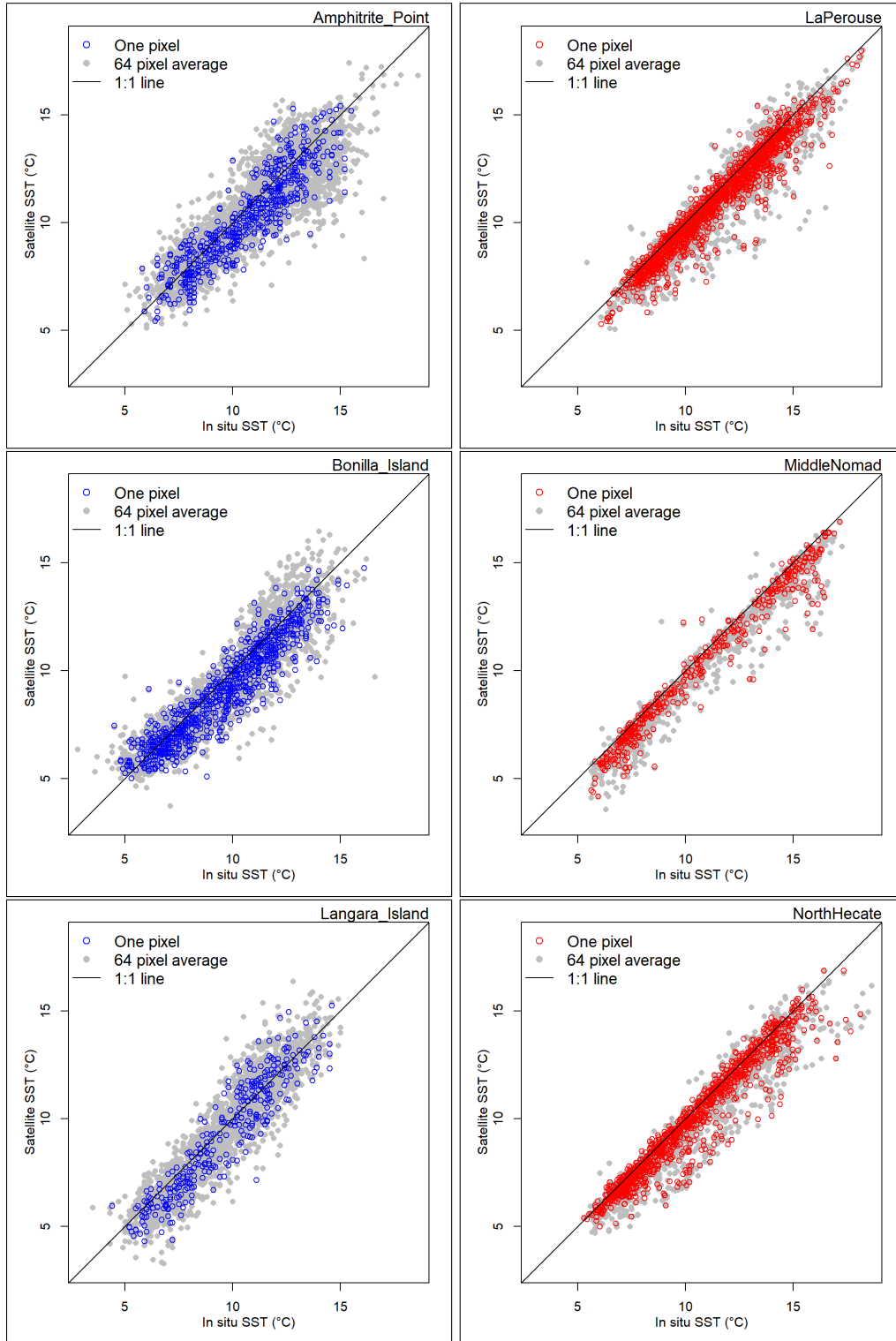


Figure 6: Satellite SST versus *in situ* SST for the three light stations (Amphitrite Point, Bonilla Island, and Langara Island) and three buoys (LaPerouse, Middle Nomad, and North Hecate). Light stations are indicated by blue solid circles (left column) and buoys are indicated by red open circles (right column).

Table 7: The mean absolute error (MAE), mean absolute percent error (MAPE), mean relative error (MRE), and mean relative percent error (MRPE) for buoys: La Perouse (LP), Middle Nomad (MN), and North Hecate (NH).

Site	Pixels	MAE ($^{\circ}\text{C}$)	MAPE (%)	MRE ($^{\circ}\text{C}$)	MRPE (%)
LP	One	0.56	4.95	-0.47	-4.10
	3x3	0.59	5.12	-0.48	-4.20
	5x5	0.61	5.33	-0.50	-4.35
	6x6	0.62	5.43	-0.51	-4.42
	8x8	0.64	5.61	-0.51	-4.45
MN	One	0.58	5.67	-0.53	-5.21
	3x3	0.60	6.10	-0.56	-5.72
	5x5	0.60	6.12	-0.57	-5.76
	6x6	0.62	6.30	-0.58	-5.90
	8x8	0.62	6.20	-0.58	-5.81
NH	One	0.51	4.93	-0.41	-3.96
	3x3	0.56	5.45	-0.49	-4.72
	5x5	0.58	5.63	-0.51	-4.90
	6x6	0.59	5.74	-0.51	-4.95
	8x8	0.61	5.94	-0.52	-5.12

Table 8: The mean absolute error (MAE), mean absolute percent error (MAPE), mean relative error (MRE), and mean relative percent error (MRPE) for light stations: Bonilla Island (BI), Langara Island (LI), and Amphitrite Point (AP).

Site	Pixels	MAE ($^{\circ}\text{C}$)	MAPE (%)	MRE ($^{\circ}\text{C}$)	MRPE (%)
AP	One	0.84	8.02	-0.42	-3.55
	3x3	0.85	7.93	-0.39	-3.10
	5x5	0.87	7.91	-0.39	-2.99
	6x6	0.88	7.95	-0.39	-2.92
	8x8	0.90	8.15	-0.39	-2.89
BI	One	0.76	8.15	-0.49	-4.51
	3x3	0.79	8.54	-0.50	-4.32
	5x5	0.78	8.40	-0.43	-3.68
	6x6	0.77	8.29	-0.35	-2.97
	8x8	0.77	8.23	-0.31	-2.54
LI	One	0.81	8.71	-0.32	-3.92
	3x3	0.77	8.41	-0.21	-2.54
	5x5	0.75	8.32	-0.13	-1.70
	6x6	0.75	8.36	-0.16	-2.11
	8x8	0.76	8.49	-0.19	-2.54

This is the case of the North Hecate buoy; *in situ* measurements show higher temperatures of about 1 to 2 $^{\circ}\text{C}$ compared to satellite measurements (Pathfinder AVHRR) in the spring of 2018 (Figure 7). Satellite and *in situ* buoy measurements agreed again in summer 2019 for a few weeks, until marked difference occurred again and continued through the rest of 2018 and 2019. This discrepancy is further highlighted when we compare the 2018 and 2019 data to the rest of the time series (8). From 1998 to 2017, there is a good agreement between the satellite and buoy data which spread along the one-to-one line. Early 2018, there is a good agreement between the satellite and *in situ* data. This is followed by an abrupt increase *in situ* temperatures. The biases appeared to be linear and could be a constant shift in the buoy measurements. The results show

that satellite-derived SST can provide a rapid assesment of buoy status and help detect anomalies due to instrument failure.

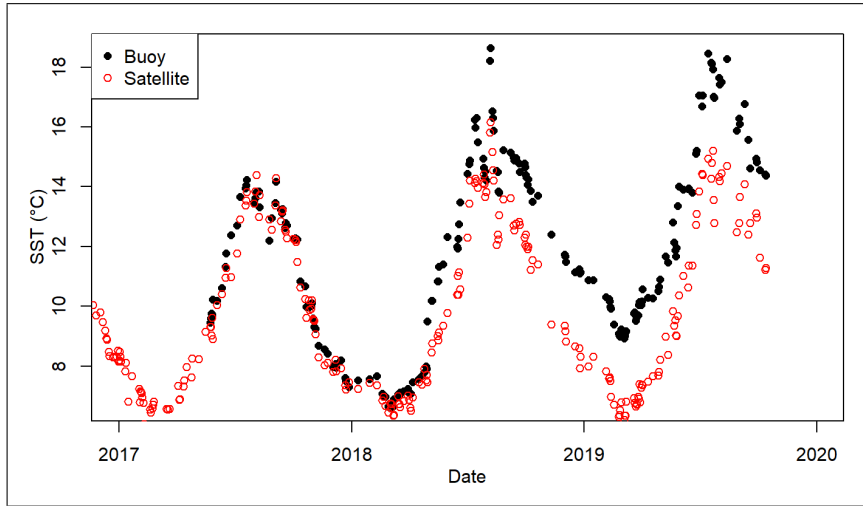


Figure 7: Daily satellite SST timeseries for North Hecate weather buoy with a focus on 2018-2019.

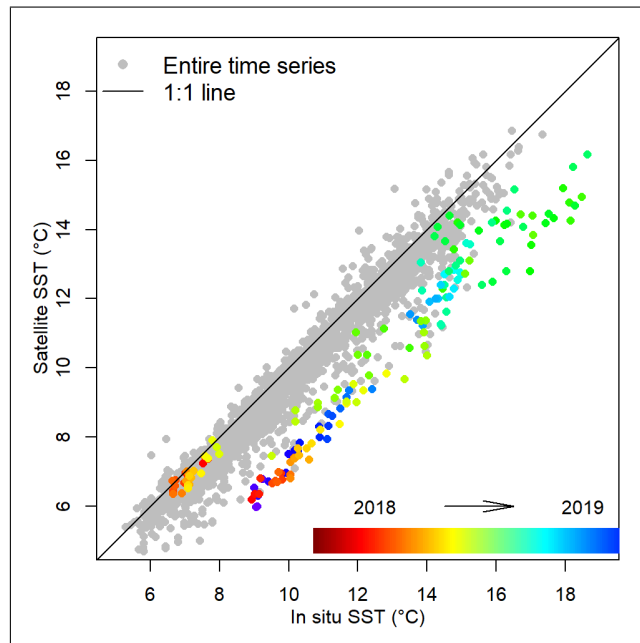


Figure 8: Satellite versus *in situ* SST North Hecate weather buoy for 2018 and 2019. Grey circles correspond to the 1988-2017 timeseries. Coloured circles correspond to 2018-2019 timeseries. The solid black line corresponds to the 1:1 line.

3.2.3 Gwaii Haanas Temperature in Relation to Bonilla Island Light station

Gwaii Haanas was designated a marine conservation area reserve in 2010 given its pristine condition and rich biodiversity. Efficient management of this area requires knowledge of baseline conditions to measure the effect of climate change and the warming ocean. While satellite SST provides

information over the last four decades, the use of light station measurements would allow the opportunity to obtain information further back in time (i.e., 1960), therefore providing trends in temperature for the last 80 years. To that purpose, we investigated the relationship between satellite-derived SST at Gwaii Haanas and *in situ* temperature measured at the Bonilla Island light station.

The daily satellite-derived SST for the three regions of Gwaii Haanas (GHE, GHW, and GHS) were regressed against the satellite-derived SST for the Bonilla Island (BI) light station (Table 9). For all GH regions, the linear regression shows that with a higher BI spatial resolution (and higher data availability, as previously discussed) the slope approaches 1 and simultaneously the intercept decreases. For example, a comparison of the daily SST of GHE to the daily SST of BI with one pixel yields a slope of 0.77 ± 0.02 and an intercept of 1.55 ± 0.15 . But if we increase the size of BI to 8x8 pixels, a slope of 0.82 ± 0.01 and an intercept of 1.26 ± 0.08 is computed. For all GH regions (east, west, and south), a slope lower than one is calculated (regardless of BI spatial resolution), meaning the temperature at the BI light station is on average lower than at Gwaii Haanas.

In general, the agreement between satellite and *in situ* measurements is better at low temperatures (i.e., winter) than at high temperatures (summer), as this discrepancy in the data increases with temperature. One also observed a systematic underestimation of temperature by the satellite in summer was also observed. The good agreement in winter could be explained by the fact that mixing is stronger during this time of year such that the water may be more homogeneous over a large area than in summer. In addition, local thermal effects in the nearshore environment in summer (e.g., sun radiation warming dark rocks) could increase the difference between the Gwaii Haanas site and the Bonilla Island light station. This information should be taken into account, and seasonal biases accounted for, when extending the BI light station temperature to the Gwaii Haanas area.

Table 9: Linear regression of Bonilla Island (BI) satellite SST data versus Gwaii Haanas (GH) satellite SST data for the three regions: GHE, GHS, and GHW. RSE is the residual standard error and N is the number of observations (days where BI and GH regions both have data).

Note: ** p-value < 0.01 and * p-value < 0.1

Site	Pixels (BI)	Slope	SE	Intercept	SE	RSE	N
GHE	One	0.77**	0.02	1.55**	0.15	0.94	620
	3x3	0.76**	0.01	1.62**	0.11	0.93	1144
	5x5	0.78**	0.01	1.48**	0.10	0.94	1489
	6x6	0.8**	0.01	1.34**	0.09	0.95	1691
	8x8	0.82**	0.01	1.26**	0.08	0.94	1873
GHW	One	0.81**	0.01	1.09**	0.13	0.80	617
	3x3	0.8**	0.01	1.14**	0.09	0.80	1164
	5x5	0.81**	0.01	1.08**	0.09	0.82	1456
	6x6	0.84**	0.01	0.86**	0.08	0.83	1627
	8x8	0.85**	0.01	0.81**	0.08	0.82	1778
GHS	One	0.8**	0.01	1.15**	0.15	0.86	600
	3x3	0.77**	0.01	1.33**	0.11	0.88	1112
	5x5	0.78**	0.01	1.28**	0.10	0.90	1432
	6x6	0.81**	0.01	1.1**	0.09	0.91	1620
	8x8	0.82**	0.01	1.03**	0.08	0.90	1789

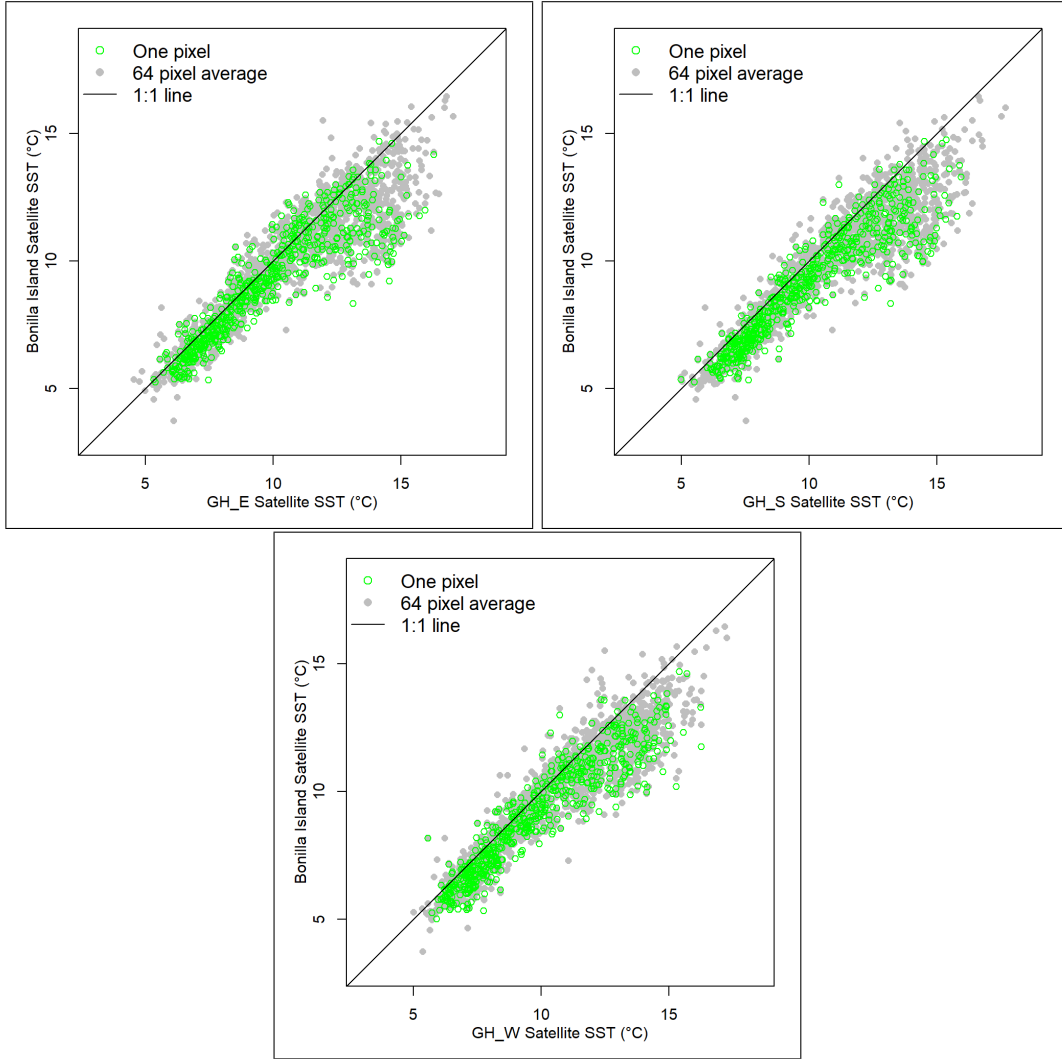


Figure 9: Correlation plot of the daily mean satellite-derived SST for all Gwaii Haanas regions versus Bonilla Island at various spatial resolutions.

3.2.4 Climatology and seasonal cycle at the synoptic scale

An important aspect of baseline conditions for a given area is the knowledge of seasonal cycles for any given properties. Comparison of any given year to its climatology (i.e., seasonal cycle) provides information on the health of the ecosystem and assists with decision making. The seasonal cycle for SST follows a sinusoidal cycle with low temperatures in the winter reaching a minimum of about 8°C at around week 10. Temperatures start to rise in late winter and continues to rise through early spring to reach a maximum of ~ 16°C around week 35 in the summer. After week 35, temperatures decrease monotonically to the winter minimum. The seasons with the greatest range of temperature were observed to be in spring and fall (Figure 10).

The seasonal cycle for CHLA shows a more variable pattern than SST, with a succession of peaks that occur between week 8 and week 40. The maximum concentration of about 1.6 mg m⁻³ is reached on week 19 and could be considered as the main feature of the spring bloom. However, given the highly temporal variability of the spring bloom, for which all the controlling

parameters are not fully understood yet, the climatology indicates that the spring bloom can also occurs earlier or later than week 19 and as late as week 30 with a chlorophyll-a concentration of 1.4 mg m^{-3} (Figure 10). It is noteworthy that spring blooms occur when SST increases, which is an indicator of the onset of stratification that traps phytoplankton in the surface layer. When this layer is exposed to sufficient light, exponential growth begins. Late fall and early winter show the lowest CHLA concentration ($\sim 0.4 \text{ mg m}^{-3}$); this is in agreement with cool sea-surface temperature limiting primary production.

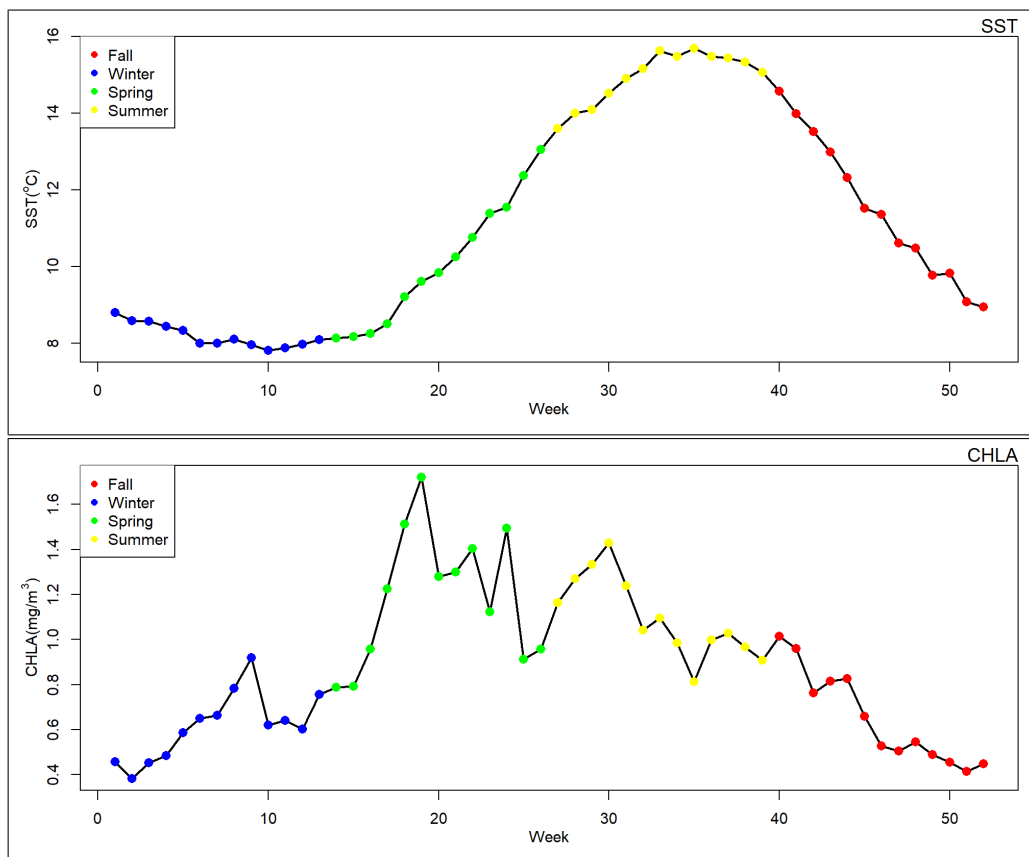


Figure 10: Weekly climatology of SST (top, 1981-2019) and CHLA (bottom, 2003-2019) for the entire region of interest. Blue, green, yellow, and red solid circles correspond to winter, spring, summer, and fall seasons respectively.

3.3 Environmental indices

3.3.1 Time series and trend analysis

To detect any significant trends we used a linear regression of monthly mean SST and CHLA. A linear regression was selected over more advanced methods as it provides a fast and robust indication of possible trends. The linear regression on the entire time series of SST in each region did not provide any significant trends, but when seasonal data were considered, some significant trends emerged. Only winter shows a significant positive trend ($p\text{-value} \leq 0.05$) in all regions, with slopes ranging between 0.15 ± 0.07 (in GHW) to 0.26 ± 0.07 (in SK-B). In summer, all regions except GHE and GHS showed significant positive trends, with slopes ranging from 0.28 ± 0.10 (in

SK-B) to 0.33 ± 0.08 (in AOI). Spring and fall did not show any significant trends, except for the SI area in fall with a p-value of 0.062 and a slope of 0.22 ± 0.12 which can be explained by the high variability in the timing of warming or cooling, of the water column due to onset of stratification (in summer) or mixing by atmospheric forcing (in fall), respectively. Table 10 shows the values for the slope and p-values (indicated by '*' or '**') for all regions.

Table 10: Summary of slope (C° /decade), standard error (C°), and p-value for the seasonal linear regression in each subregion.

Note: ** p-value < 0.01 and * p-value < 0.1

Site	Season	Slope	SE	Intercept	SE
AOI	Winter	0.25**	0.06	7.15**	0.21
	Spring	0.19	0.15	9.14**	0.48
	Summer	0.33**	0.08	14.21**	0.27
	Fall	0.23	0.17	11.13**	0.58
SK-B	Winter	0.26**	0.07	5.55**	0.21
	Spring	0.13	0.15	7.58**	0.48
	Summer	0.28**	0.10	12.67**	0.34
	Fall	0.2	0.15	8.87**	0.52
GHE	Winter	0.24**	0.08	6.43**	0.23
	Spring	0.16	0.15	8.62**	0.47
	Summer	0.07	0.10	13.3**	0.30
	Fall	0.16	0.12	9.22**	0.37
GHW	Winter	0.15*	0.07	6.87**	0.26
	Spring	-0.01	0.11	8.86**	0.39
	Summer	0.28**	0.09	12.3**	0.30
	Fall	0.14	0.13	9.47**	0.46
GHS	Winter	0.2**	0.07	6.72**	0.23
	Spring	0.07	0.13	8.91**	0.41
	Summer	0.12	0.09	13.14**	0.27
	Fall	0.15	0.12	9.42**	0.39
SI	Winter	0.23**	0.07	7.11**	0.22
	Spring	0.19	0.14	9.34**	0.45
	Summer	0.3**	0.08	12.81**	0.24
	Fall	0.22*	0.12	9.87**	0.41

The three offshore areas (AOI, SK-B, and SI) show the highest rates of warming in the summer and winter. In winter, SK-B and AOI show slope values of 0.25 ± 0.06 and 0.26 ± 0.07 , respectively. In summer, AOI and SI show slope values of 0.33 ± 0.08 and 0.30 ± 0.08 , respectively. For the coastal areas of Gwaii Haanas (GHE, GHW, and GHS), the eastern part of Gwaii Haanas (GHE) has a highest rate of warming in the winter with a slope of 0.24 ± 0.08 while the southern (GHS) and western (GHW) regions show lower rates with slopes of 0.20 ± 0.07 and 0.15 ± 0.07 , respectively. For summer, GHW has the highest rate of warming and the only significant trend in the summer for coastal areas with a slope of 0.28 ± 0.09 . The summer rate of warming over the 41 years of observations was higher (when significant) than for the rate for winter. The time series of SST in all regions show the warm event that occurred in 2015; this is when a strong positive anomaly occurred in the Northeast Pacific (Bond et al., 2015). Figures 11 and 12 shows the monthly time series for all regions.

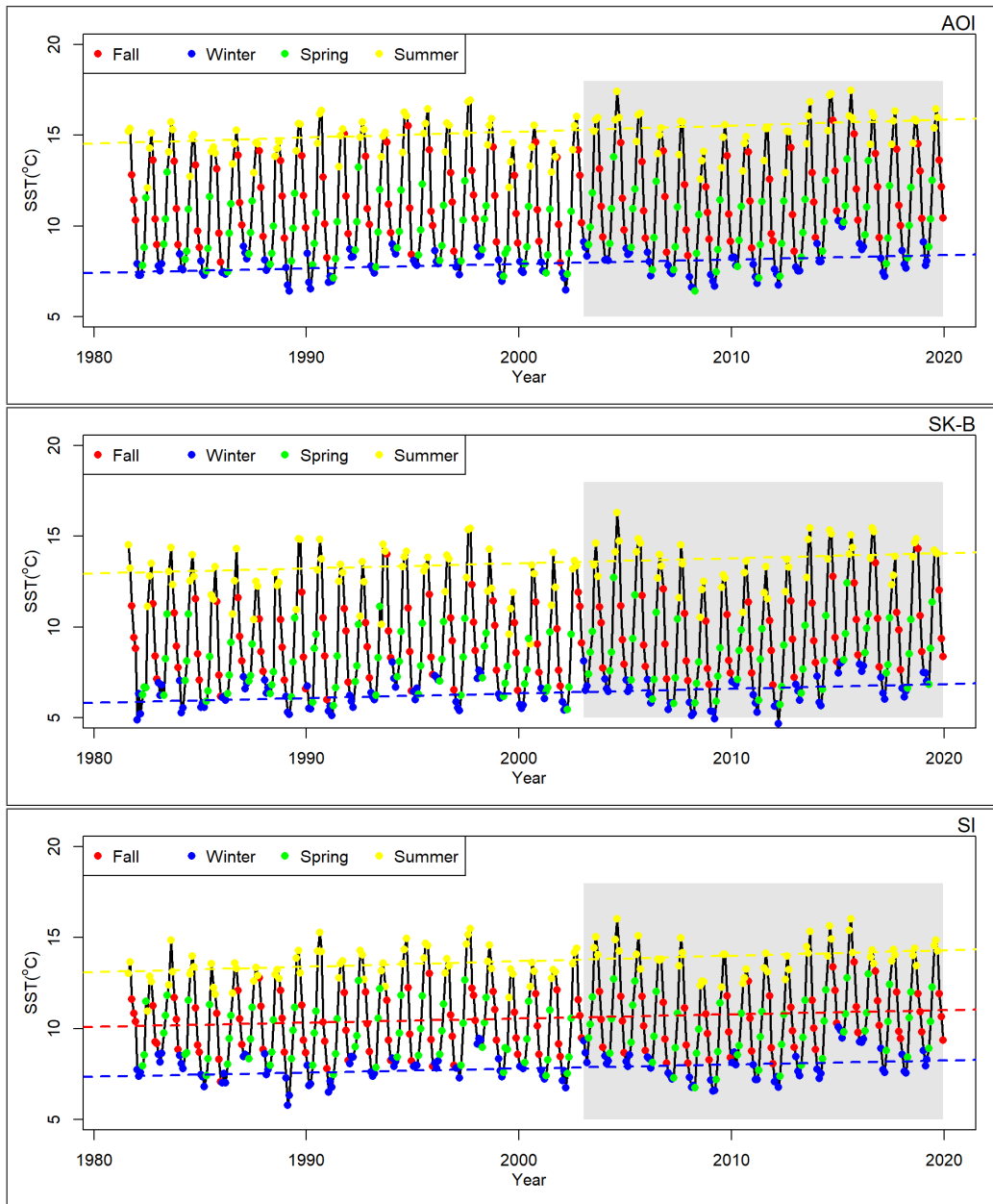


Figure 11: Monthly mean SST time series for AOI, SK-B, and SI between August 1981 and September 2019. Dashed lines indicate linear regression with a significant trend ($p\text{-value} \leq 0.05$) for a given season fall (red), winter (blue), spring (green), and summer (yellow). The grey shaded areas represent the common time coverage between SST and CHLA.

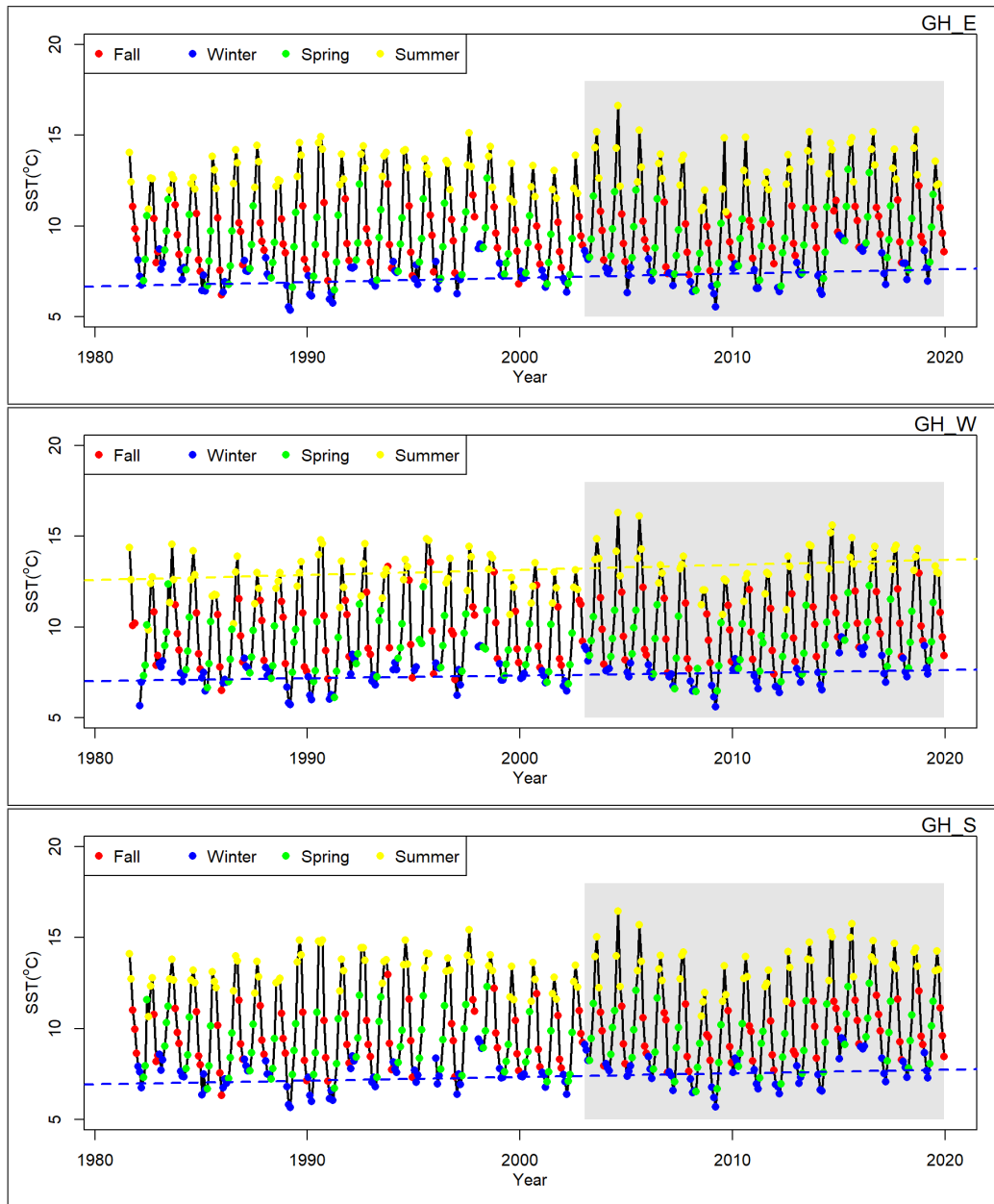


Figure 12: Monthly mean SST time series for the Gwaii Haanas regions between August 1981 and September 2019. East (top), west (middle), and south (bottom). The gray shaded areas represent the common time coverage between SST and CHLA.

For CHLA, the climatology of the entire region revealed a succession of peaks from week 10 to about week 40. The time series for individual regions of interest show a high variability in timing and intensity of phytoplankton bloom, supporting the need to account for regional characteristics. As for the seasonal cycle, the CHLA time series shows a very different pattern than the SST time series with greater variability in magnitude and timing of maximum.

The offshore areas (AOI, SK-B, and SI) show the lowest chlorophyll-a concentration on average with values ranging from 0.2 to 3.0 mg m⁻³ (Figure 13). Scott Islands NWA (SI) shows a larger

CHLA concentration compared to the other offshore areas, possibly due to its closer proximity to the shore and that half its surface area is located on the shelf, where CHLA concentration is generally higher than in the oligotrophic deep basin. The coastal area of Gwaii Haanas recorded the highest CHLA, with values up to 7.5 mg m^{-3} in the eastern area (GHE). In 2009 CHLA was abnormally high in all three region of Gwaii Haanas, with values of 7.5, 6.2 and 4.2 mg m^{-3} for the east, west, and south region, respectively (Figure 14). This abnormally high CHLA corresponds to a relatively cold year of SST during the same period (i.e., 2003 to 2019, Figure 12). Interestingly, peaks of CHLA occur in the fall in the AOI and SK-B region, suggesting that mixing might be an important factor to replenishing the upper layer of the ocean with nutrients where light levels are still sufficient at this time of the year to support phytoplankton growth. Following the fall, the second season of high chlorophyll-a concentration is in the spring as expected.

In the SI region, the spring bloom represents the major event in phytoplankton biomass followed by the summer. The chlorophyll-a dynamic is different in the three Gwaii Haanas regions, where the spring season had the highest CHLA concentration from 2003 to about 2009 (Figure 13). Following that period, highest chlorophyll-a concentrations were observed in summer until 2015, when spring was again the season where chlorophyll-a concentration was highest. This pattern is consistent with sea-surface temperature for the same period (Figure 11) where we observed decreasing SST from 2003 to 2009 followed by increasing SST from 2010 to 2015 where a new decrease was observed again until 2019. These results illustrate the strong relationship between physical forcing and the biological response at low temporal resolution (monthly data), and inform on the potential use of SST to infer the timing and magnitude of the "spring" phytoplankton bloom.

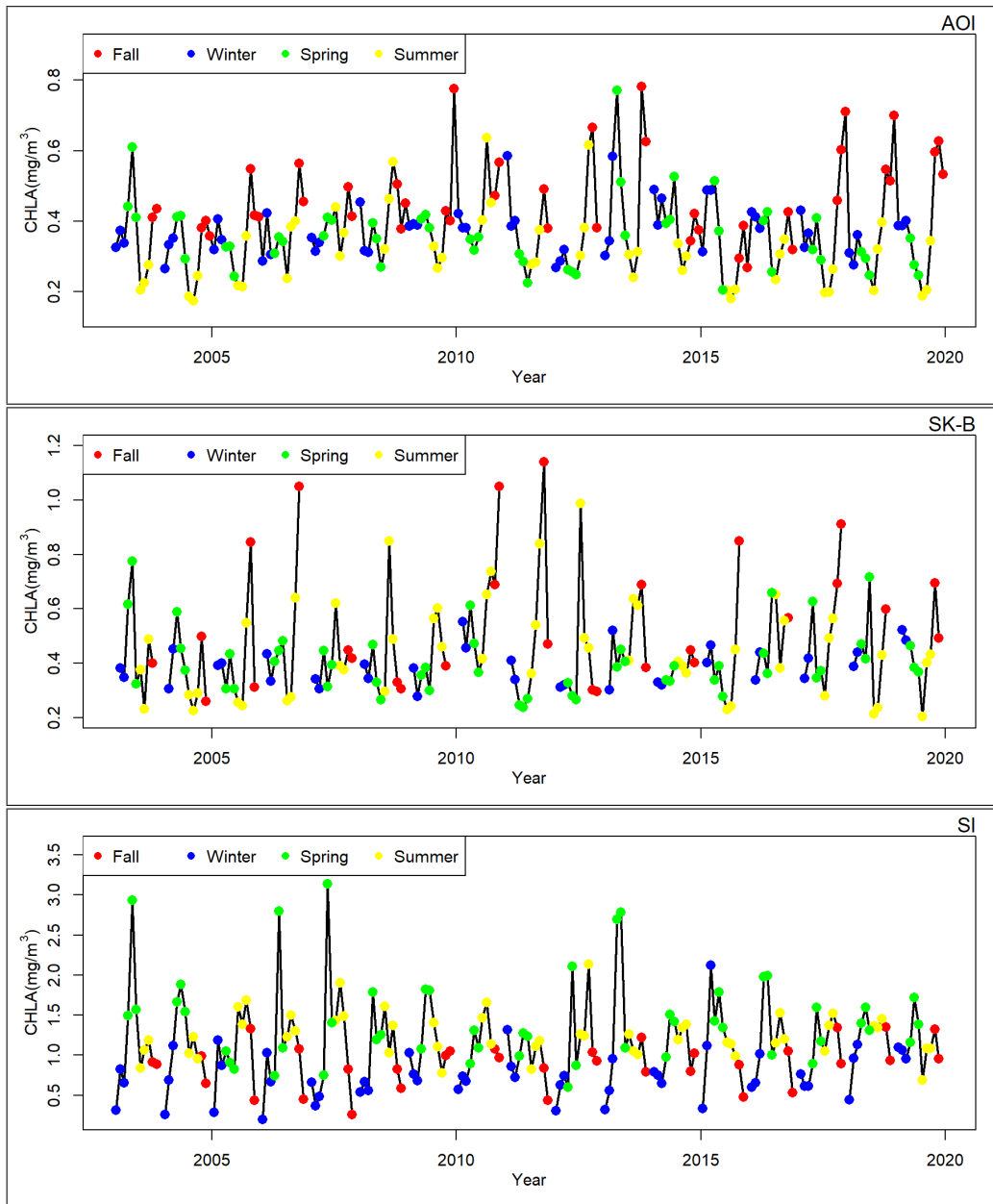


Figure 13: AOI, SK-B, and SI monthly time series for CHLA from January 2003 to December 2019. Blue, green, yellow and red solid circles correspond respectively to winter, spring, summer and fall season.

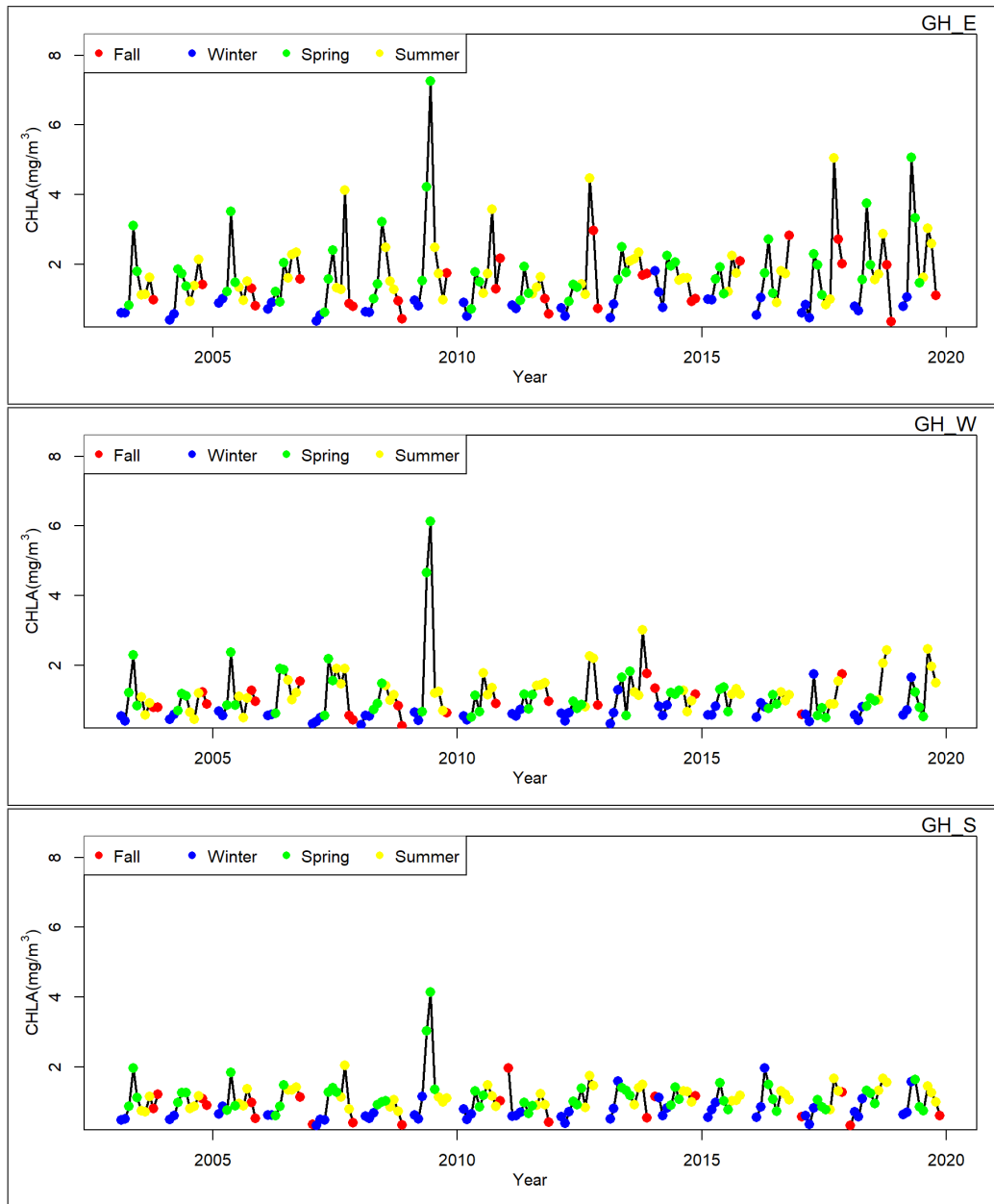


Figure 14: Gwaii Haanas regions monthly time series for CHLA from January 2003 to December 2019. East region (top), west region (middle), and south region (bottom). Note that for these plots, the y-axis was adjusted to be the same range to show the difference in CHLA concentration in each Gwaii Haanas region.

3.3.2 Number of days with SST ≥ 11 in Gwaii Haanas

A kelp forest, which provides ecosystem services in the nearshore environment, is sensitive to sea temperature and notably warming of the ocean. A study showed that kelp forests in coastal British Columbia suffered loss from the marine heatwave that reached the shore in 2014-2016 when compared to distribution of kelp during 1993-1995 (Starko et al., 2019). An index to inform on the possible impact of temperature on kelp health is to study the phenology of sea-surface temperature and notably the number of days over a given temperature threshold, here we selected a threshold of

11°C. We focused the study on the Gwaii Haanas, which hosts large areas of kelp forest that have been under pressure from seawater warming and grazers. The daily SST data for Gwaii Haanas were interpolated due to gaps in the time series (Figure 15). Out of 13850 possible days (over 41 years), 2299 had a data coverage $\geq 10\%$, interpolation provided a mean to obtain a time series without gaps to determine the number of consecutive days where SST was $\geq 11^\circ\text{C}$.

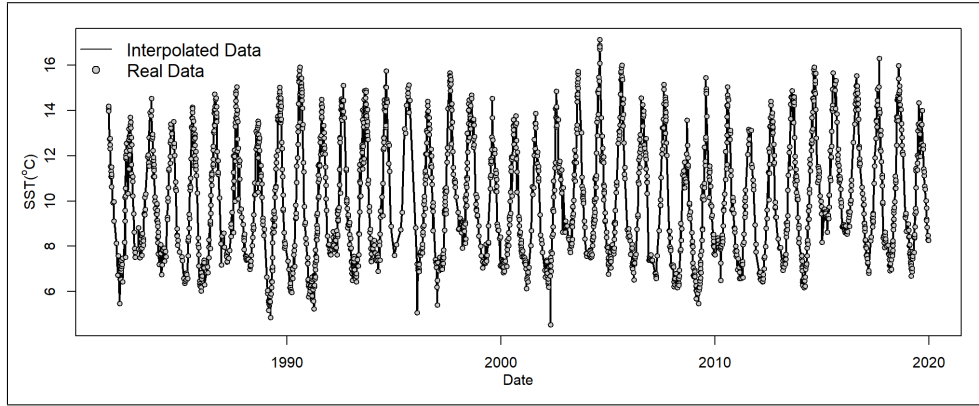


Figure 15: Interpolated daily SST data for the Gwaii Haanas area (west, east, and south combined). The 'real data' show the points the interpolation was based on.

The number of days with sea-surface temperature $\geq 11^\circ\text{C}$ varies between 81 (2008) and 174 (1995) (Table 11). The year 1995 appeared to be an exceptionally warm year, however, 2014 to 2016 saw consecutive years with more than 155 days $\geq 11^\circ\text{C}$. This is in agreement with the average increase in the number of days $\geq 11^\circ\text{C}$ for the last four decades at a rate of approximately 0.76 days per year (Figure 16, p-value of 0.02). While some years saw a continuous period of year above the threshold (e.g., 2005, 2006, 2016, and 2019), other years have seen a succession of periods with temperature over 11°C interrupted by periods of cooler temperatures (e.g., 2008 and 2013). The impacts of the variations in SST on the coastal ecosystem should be studied. Finally, the first day of year above 11°C did not show any significant trends for any of the three regions of Gwaii Haanas.

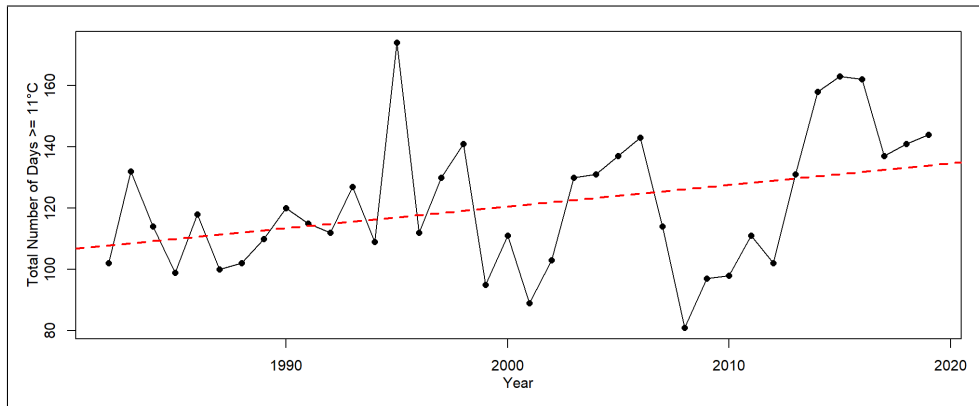


Figure 16: The total number of days where the mean SST was $\geq 11^\circ\text{C}$ for Gwaii Haanas. Note this is based on interpolated data as the daily data availability alone would not be sufficient.

Table 11: Consecutive days where SST was above or below 11 deg in Gwaii Haanas.

Year	Number of Days SST Temperature								Total Days		
	<11°C	≥11°C	<11°C	≥11°C	<11°C	≥11°C	<11°C	≥11°C	<11°C	≥11°C	
1982	163	32	15	68	3	2	78			259	102
1983	157	132	74							231	132
1984	168	114	81							249	114
1985	177	1	2	98	84					263	99
1986	169	7	7	111	70					246	118
1987	179	10	2	10	5	55	4	25	75	265	100
1988	191	42	1	5	1	55	69			262	102
1989	173	2	4	108	78					255	110
1990	164	120	81							245	120
1991	170	4	10	111	70					250	115
1992	165	17	3	95	85					253	112
1993	145	9	15	118	78					238	127
1994	181	109	75							256	109
1995	156	174	35							191	174
1996	171	112	83							254	112
1997	166	130	69							235	130
1998	149	5	1	136	74					224	141
1999	187	86	5	9	77					269	95
2000	172	16	6	75	5	20	72			255	111
2001	191	79	1	10	82					274	89
2002	186	100	19	3	57					262	103
2003	154	15	2	113	4	2	74			234	130
2004	150	4	11	127	73					234	131
2005	155	137	73							228	137
2006	159	143	63							222	143
2007	175	114	76							251	114
2008	181	20	3	4	8	17	9	40	84	285	81
2009	184	81	5	6	1	10	78			268	97
2010	181	98	86							267	98
2011	174	111	80							254	111
2012	182	6	5	96	77					264	102
2013	159	113	1	8	5	7	6	3	63	234	131
2014	159	136	3	16	1	6	43			206	158
2015	139	6	2	146	1	4	4	7	54	200	163
2016	142	162	58							200	162
2017	165	136	3	1	60					228	137
2018	160	2	6	139	57					223	141
2019	146	144	75							221	144

3.3.3 Marine heatwave in 2018-2019

Global warming is affecting our oceans and the temperature of the global ocean is increasing, perhaps at accelerating rates (Iz, 2018). One of the major manifestation of the ocean warming is the occurrence of marine heatwaves, which happen when large bodies of seawater with abnormally high temperatures spread over large areas for several months and can drastically impact the marine ecosystem (e.g., coral bleaching and mass mortality). These alarming events have gathered the scientific community in international working groups to monitor these events (for more information, see: <http://www.marineheatwaves.org/>). For instance, in 2014-2015 an unprecedented heatwave

hit the Northeast Pacific, including British Columbia, with negative effects on the marine ecosystem such as mass mortality, invasion of foreign species, decrease in primary production and occurrence of harmful algal events (Crozier, 2015).

Here, we used the Pathfinder AVHRR satellite data to follow a heatwave that started in 2018 and continued to 2019. The objective was to find appropriate temporal and spatial binning to provide informative data to the science branch at the Institute of Ocean Sciences and define a product that could be useful for management. It seems that 4 km resolution is suitable to track the marine heatwave in the coastal environment, compared to the quarter of a degree resolution used by the marine heatwave international working group. Temporal binning appeared to be critical (Figure 17). While 8-day composite images averaged over a spatial area seemed appropriate for time series analysis for our region of interest, monthly composites seemed more suitable on a pixel-per-pixel based analysis.

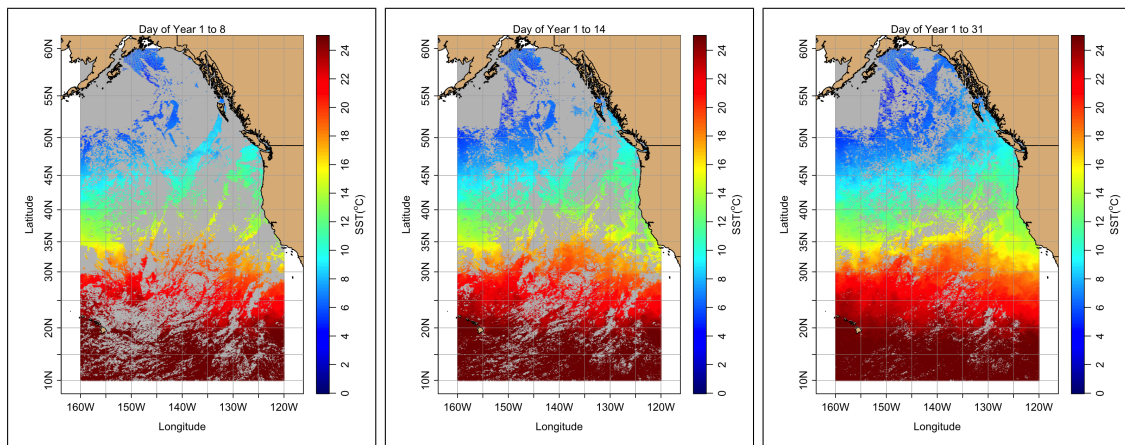


Figure 17: Comparison of coverage for the different SST composites in 2018: 8-day composite (left), 14-day composite (middle), and monthly composite (right).

First, monthly composites were computed for a reference period that spanned years 1990 to 2003 (Figure B.1). There is a difference between the Southern (warm) and Northern (cold) regions of the Northeast Pacific that occurs around 35° North. Starting in June, there is warm water progressing along the North American coast all the way to Alaska, reaching a maximum temperature in August. In summer 2018 and 2019, the warm waters extend much further over the entire Northeast Pacific with maximum temperatures in the $18\text{-}20^{\circ}\text{C}$ range, while the maximum is around $16\text{-}18^{\circ}\text{C}$ in the climatology. A similar pattern is also observed in the Fall and Winter with warmer water during 2018-2019 than in the reference period. This is evidenced when looking at the anomalies (Figures 18, B.2 and B.3). For instance, in October 2018 the positive anomalies, as indicated by the red areas, are as high as 5°C and spread throughout the entire northern part of the Northeast Pacific, including the Canadian shore; the coast of Alaska recorded the highest temperature.

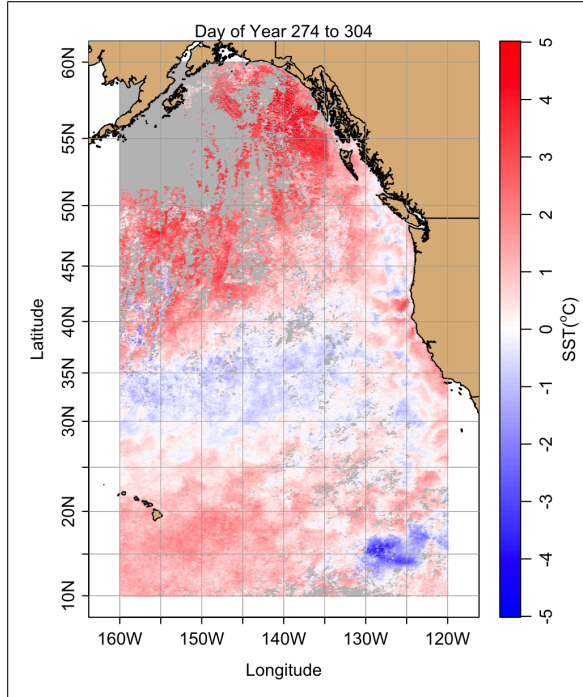


Figure 18: SST Anomaly for the month of October 2018

3.3.4 Cumulative CHLA

The large variations in the number, intensity, and timing of phytoplankton growth events do not allow for the use of classical methods to characterize the spring bloom and therefore determine useful metrics to inform on phytoplankton dynamics in the Northeast Pacific (Siegel et al., 2002; Zhai et al., 2011; Brody et al., 2013). Here we tested if cumulative chlorophyll-a concentration could provide an insight in the dynamics of primary producers (Figure 19). Cumulative CHLA is about three times higher in coastal areas (i.e., GH regions and SI) than in pelagic areas (i.e., AOI and SK-B). For example, the total cumulative CHLA in GHE ranges from 387 to 752 mg m^{-3} while cumulative CHLA in AOI ranges from 117 to 173 mg m^{-3} (Table 12). The total cumulative CHLA concentration provides an insight into the standing stock of phytoplankton biomass of this region and informs on the potential support to higher trophic levels of these ecosystems. It is noteworthy that the Gwaii Haanas east region has the highest mean cumulative CHLA which is 40% and 60% higher than the southern and western regions, respectively.

Table 12: The mean, minimum, and maximum cumulative total (mgm^{-3}) in each region.

Region	Mean	Min	Max
AOI	137	117	173
SK-B	162	137	228
GHE	568	387	752
GHS	350	260	442
GHW	393	291	629
SI	416	355	561

With the coastal regions having a higher cumulative CHLA total than offshore (pelagic)

regions, a cumulative threshold of 100 mg m^{-3} was assigned for coastal regions (i.e., GH regions and SI) and 50 mg m^{-3} for offshore regions (i.e., AOI and SK-B). For Gwaii Haanas, GHE reaches the cumulative threshold, which roughly corresponds to a quarter of the annual cumulative CHLA, on average on day 115 while GHW and GHS reach this threshold on average on day of year 136 and 132, respectively. For the SI region, this threshold on average was reached slightly earlier than for the GH regions on day of year 116. For AOI and SK-B, the threshold was reached on average on day of year 133 and 125, respectively, which are similar values to those recorded for the coastal areas. Interannual variation is quite large (50 days for the SI region to 80 days for GHE). Coastal regions show abrupt increases of cumulative CHLA around day of year 150 while the increase presents a more monotonous pattern for the offshore areas. The year 2008 was an exceptional year with an early and sudden increase in CHLA in the Gwaii Haanas MPA (Figure 19). The GHE region is the only region that showed a significant negative slope (slope of 0.31 and $p\text{-value} < 0.01$), meaning that the threshold of 100 mg m^{-3} is reached three days earlier each year over the period of observation.

Table 13: The first day where cumulative CHLA reaches the threshold. Where the thresholds are 50 mgm^{-3} (AOI and SK-B) and 100 mgm^{-3} (GH regions and SI).

Year	AOI doy	SK-B doy	GHE doy	GHS doy	GHW doy	SI doy
2003	139	132	131	147	129	123
2004	138	125	124	126	137	110
2005	140	129	120	125	127	117
2006	152	126	135	153	137	100
2007	137	125	143	158	138	134
2008	129	119	143	160	151	116
2009	124	162	119	137	141	128
2010	128	101	133	130	168	134
2011	104	112	117	100	137	107
2012	179	152	140	151	140	136
2013	105	135	113	114	125	110
2014	116	149	82	103	107	126
2015	121	124	63	127	129	67
2016	127	130	115	115	151	116
2017	141	112	96	143	109	135
2018	158	98	90	132	152	114
2019	130	93	95	128	126	95
Average	133	125	115	132	136	116

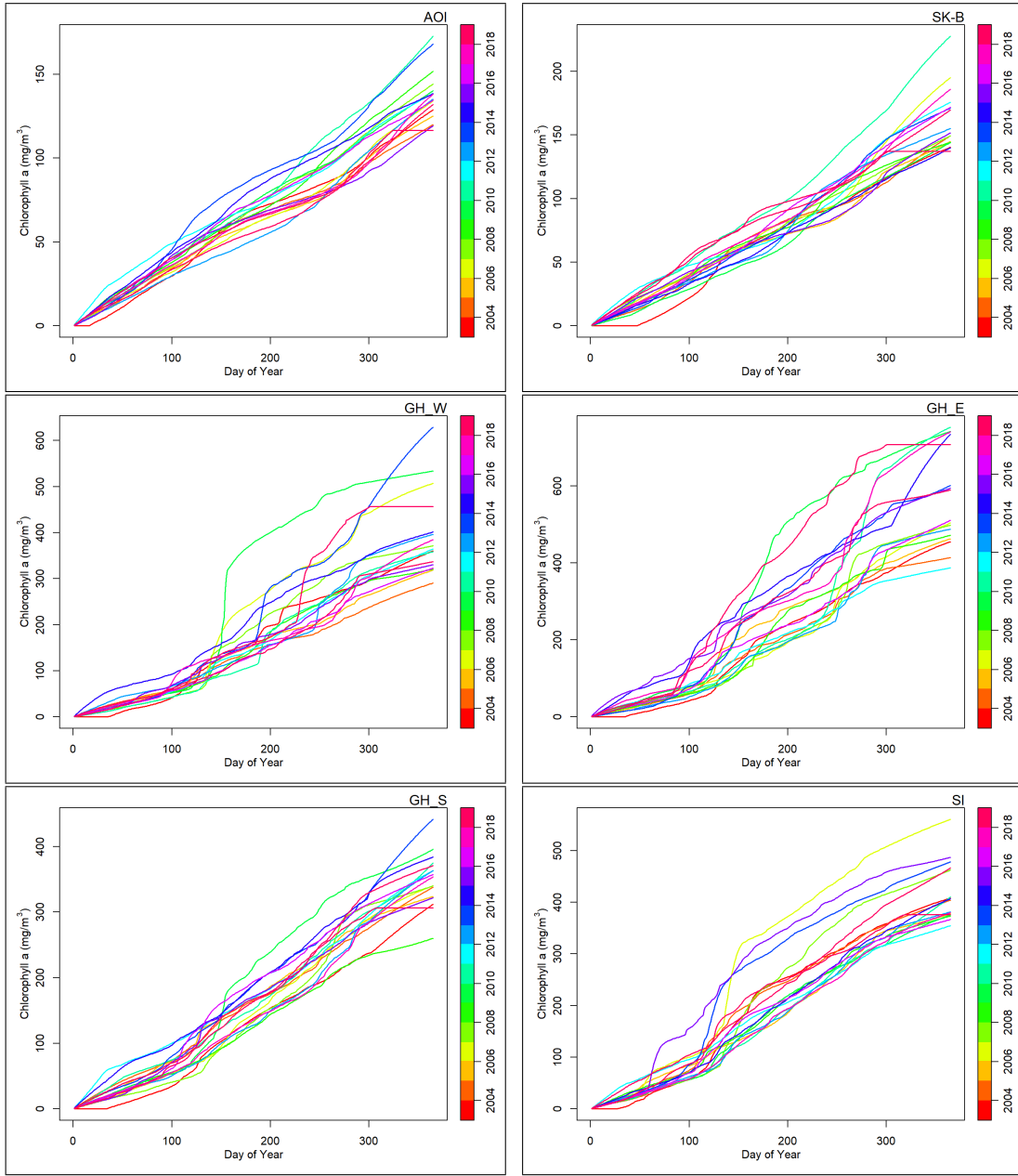


Figure 19: Cumulative CHLA based on interpolated CHLA daily geometric mean from 01/01/2003 to 31/12/2019 for each region.

4 Conclusion

The current study presented a suite of products to determine baseline conditions of chlorophyll-a concentration and sea-surface temperature and quantify their changes over several decades in the Northeast Pacific, in particular in six areas of interest to DFO. This study showed that cloud cover has a strong impact on temporal and spatial distribution of satellite measurements, and missing data may vary between 60 and 100% of any given temporal or spatial binning. As expected, the smaller the study area, the higher the number of days or weeks without data, such that careful

considerations are required before carrying out data analysis. Methods to fill missing data have been tested in the region, such as the data interpolating empirical orthogonal functions (DINEOF) (Hilborn and Costa, 2018; Liu and Wang, 2019).

Four metrics were tested to assess the health of the six regions of interests (EHV excluded). Sea-surface temperature seasonal cycle (i.e., climatology) exhibited a common sinusoidal pattern that peaks in the summer, while chlorophyll-a concentration showed variable seasonal cycles with a succession of peaks. Sea-surface temperature has been increasing in winter for all the regions of interest, while such conclusions were not evidenced for the other seasons except for the Scott Islands NWA in Fall and Summer. No trends were found for chlorophyll-a concentration except for the GHW region in Fall, which has significantly increased during the 17 years of observation. The number of days of SST greater than 11°C was counted for the entire Gwaii Haanas MPA and revealed a significant increase over the last 4 decades at a rate of 0.766 day/year. This phenomenon will have drastic effects on the coastal marine habitat. Regarding SST, a processing chain was developed to generate monthly anomalies computed against the 1990-2003 reference period. These images would be at the basis of a regional system to track marine heatwaves and the years 2018-2019 were selected as an illustration. While this appears to be an interesting tool, the final products may require further spatial binning; however in the current state, it would offer the possibility to zoom in on coastal areas. Finally, we computed the cumulative CHLA for the six regions of interest, which revealed that the coastal regions had annual standing stocks of phytoplankton biomass of about 3 times the ones in the pelagic regions. It is important to note that this may partly be explained by the contamination of the signal by dissolved organic matter occurring in higher concentration in coastal environments than in open waters. Coastal regions were also more subject to abrupt increases in chlorophyll-a concentration whereas pelagic region showed monotonic increases. Interestingly, all regions reached the 25% concentration around the same time (day of year 130), however, large interannual variation of about two months existed. Only one region, GHE showed a significant negative trend for the day of year when cumulative CHLA reaches 25% of annual cumulative CHLA, meaning that this threshold was achieved 30 days earlier on average per decade. While cumulative CHLA provides a preliminary insight into the functioning and phytoplankton annual standing stocks, the next step would be to compute primary production to infer carbon stocks and the amount of energy that is available for higher trophic levels.

Acknowledgement

This work was supported by DFO Strategic Program for Ecosystem-based Research and Advice funded under the project: "Satellite-based ecological indicators for the Northeastern Pacific Ocean". We thank Chantelle Layton and Stephanie Clay for programming support.

REFERENCES

- Barnes, B. B. and Hu, C. (2016). Dependence of satellite ocean color data products on viewing angles: A comparison between SeaWiFS, MODIS, and VIIRS. *Remote Sensing of Environment*, 175:120–129.
- Bond, N. A., Cronin, M. F., Freeland, H., and Mantua, N. (2015). Causes and impacts of the 2014 warm anomaly in the NE pacific. *Geophysical Research Letters*, 42(9):3414–3420.
- Brewin, R. J. W., de Mora, L., Billson, O., Jackson, T., Russell, P., Brewin, T. G., Shutler, J. D., Miller, P. I., Taylor, B. H., Smyth, T. J., et al. (2017). Evaluating operational AVHRR sea surface temperature data at the coastline using surfers. *Estuarine, Coastal and Shelf Science*, 196:276–289.
- Brewin, R. J. W., Smale, D. A., Moore, P. J., Dall’Olmo, G., Miller, P. I., Taylor, B. H., Smyth, T. J., Fishwick, J. R., and Yang, M. (2018). Evaluating operational AVHRR sea surface temperature data at the coastline using benthic temperature loggers. *Remote Sensing*, 10(6):925.
- Brody, S. R., Lozier, M. S., and Dunne, J. P. (2013). A comparison of methods to determine phytoplankton bloom initiation. *Journal of Geophysical Research: Oceans*, 118(5):2345–2357.
- Carswell, T., Costa, M., Young, E., Komick, N., Gower, J., and Sweeting, R. (2017). Evaluation of MODIS-Aqua atmospheric correction and chlorophyll products of Western North American coastal waters based on 13 years of data. *Remote Sensing*, 9(10):1063.
- Chandler, P. C., King, S. A., and Boldt, J. (2017). State of the physical, biological and selected fishery resources of Pacific Canadian marine ecosystems in 2016. *Can. Tech. Rep. Fish. Aquat. Sci.*, 3225:243.
- Clay, S., Peña, A., DeTracey, B., and Devred, E. (2019). Evaluation of satellite-based algorithms to retrieve chlorophyll-a concentration in the Canadian Atlantic and Pacific oceans. *Remote Sensing*, 11(22):2609.
- Cole, H. S., Henson, S., Martin, A. P., and Yool, A. (2015). Basin-wide mechanisms for spring bloom initiation: how typical is the North Atlantic? *ICES Journal of Marine Science*, 72(6):2029–2040.
- Crozier, L. (2015). Impacts of climate change on salmon of the Pacific Northwest. *Technical Review, National Marine Fisheries Service, National Oceanic and Atmospheric Administration*, page 46.
- DFO (2018). Oceanographic conditions in the Atlantic zone in 2017. *DFO Can. Sci. Advis. Sec. Sci. Advis. Rep.*, (2018/039).
- DFO (2019). Oceanographic conditions in the Atlantic zone in 2018. *DFO Can. Sci. Advis. Sec. Sci. Advis. Rep.*, (2019/034).
- Hilborn, A. and Costa, M. (2018). Applications of DINEOF to satellite-derived chlorophyll-a from a productive coastal region. *Remote Sensing*, 10(9):1449.

- Iz, H. B. (2018). Is the global sea surface temperature rise accelerating? *Geodesy and Geodynamics*, 9(6):432–438.
- Legendre, P. and Legendre, L. (2012). *Numerical Ecology*. Developments in Environmental Modelling. Elsevier.
- Liu, X. and Wang, M. (2019). Filling the gaps in ocean maps. *Eos*, 100.
- Perry, R. I. (2014). State of the physical, biological and selected fishery resources of Pacific Canadian marine ecosystems in 2013. *Can. Tech. Rep. Fish. Aquat. Sci.*, (3102):136.
- Siegel, D. A., Doney, S. C., and Yoder, J. A. (2002). The North Atlantic spring phytoplankton bloom and Sverdrup’s critical depth hypothesis. *science*, 296(5568):730–733.
- Smit, A. J., Roberts, M., Anderson, R. J., Dufois, F., Dudley, S. F. J., Bornman, T. G., Olbers, J., and Bolton, J. J. (2013). A coastal seawater temperature dataset for biogeographical studies: large biases between in situ and remotely-sensed data sets around the coast of South Africa. *PLoS One*, 8(12).
- Starko, S., Bailey, L. A., Creviston, E., James, K. A., Warren, A., Brophy, M. K., Danasel, A., Fass, M. P., Townsend, J. A., and Neufeld, C. J. (2019). Environmental heterogeneity mediates scale-dependent declines in kelp diversity on intertidal rocky shores. *PloS one*, 14(3).
- Zhai, L., Platt, T., Tang, C., Sathyendranath, S., and Hernández Walls, R. (2011). Phytoplankton phenology on the Scotian Shelf. *ICES Journal of Marine Science*, 68(4):781–791.

A Monthly bias for light station and buoy sites

Table A.3: Monthly bias Langara Island.

Month	1 Pixel		3x3 Pixels		5x5 Pixels		6x6 Pixels		8x8 Pixels	
	Int.	Slope r^2	Int.	Slope r^2	Int.	Slope r^2	Int.	Slope r^2	Int.	Slope r^2
Jan	1.66	0.70 0.43	1.15	0.79 0.39	1.55	0.75 0.42	1.11	0.81 0.48	1.77	0.70 0.39
Feb	1.68	0.68 0.32	0.89	0.84 0.55	0.70	0.86 0.58	1.50	0.73 0.41	1.53	0.72 0.44
Mar	1.41	0.67 0.58	1.18	0.74 0.59	2.01	0.63 0.49	1.79	0.65 0.49	1.55	0.68 0.51
Apr	-0.62	0.96 0.52	0.08	0.88 0.55	-0.17	0.92 0.56	0.35	0.85 0.50	0.39	0.83 0.49
May	2.40	0.64 0.28	1.49	0.76 0.45	2.13	0.68 0.42	1.66	0.74 0.45	1.51	0.76 0.46
Jun	4.41	0.52 0.22	5.00	0.47 0.16	5.47	0.43 0.18	5.01	0.48 0.22	4.15	0.56 0.23
Jul	-2.21	1.20 0.55	0.74	0.93 0.42	0.14	0.98 0.42	1.10	0.91 0.38	1.48	0.88 0.39
Aug	6.21	0.49 0.29	6.44	0.49 0.27	5.52	0.58 0.34	5.23	0.60 0.31	5.72	0.57 0.31
Sep	2.42	0.79 0.55	3.11	0.75 0.50	3.72	0.71 0.47	4.56	0.64 0.39	4.73	0.62 0.39
Oct	3.02	0.73 0.42	4.17	0.63 0.32	4.47	0.60 0.37	3.72	0.66 0.39	3.50	0.68 0.41
Nov	-1.31	1.12 0.55	1.32	0.84 0.55	1.15	0.89 0.62	1.11	0.88 0.62	1.27	0.86 0.62
Dec	3.59	0.49 0.14	2.60	0.67 0.29	2.26	0.72 0.47	2.00	0.74 0.48	2.13	0.71 0.48

Table A.4: Monthly bias Middle Nomad.

Month	1 Pixel		3x3 Pixels		5x5 Pixels		6x6 Pixels		8x8 Pixels	
	Int.	Slope r^2	Int.	Slope r^2	Int.	Slope r^2	Int.	Slope r^2	Int.	Slope r^2
Jan	-2.60	1.29 0.79	-1.58	1.14 0.74	-1.44	1.12 0.65	-0.78	1.03 0.60	-0.96	1.06 0.66
Feb	-0.78	1.04 0.73	-0.99	1.07 0.71	-0.75	1.03 0.71	-0.86	1.05 0.72	-0.85	1.05 0.72
Mar	-1.89	1.19 0.81	-1.68	1.16 0.81	-1.17	1.10 0.78	-1.09	1.09 0.79	-0.86	1.06 0.81
Apr	-0.96	1.07 0.88	-0.82	1.03 0.76	-1.09	1.07 0.79	-0.86	1.04 0.75	-0.64	1.01 0.72
May	0.13	0.91 0.76	-0.86	1.02 0.78	-0.91	1.03 0.80	-0.97	1.03 0.80	-0.83	1.01 0.79
Jun	1.76	0.77 0.54	0.25	0.91 0.72	-0.34	0.97 0.81	-0.61	0.99 0.82	0.15	0.92 0.81
Jul	2.17	0.79 0.71	1.48	0.85 0.70	0.71	0.90 0.70	1.02	0.88 0.68	1.03	0.87 0.65
Aug	0.19	0.92 0.57	0.23	0.93 0.60	0.44	0.91 0.59	0.66	0.89 0.54	0.78	0.88 0.54
Sep	2.23	0.82 0.77	1.77	0.85 0.81	1.52	0.86 0.74	1.40	0.87 0.76	1.31	0.87 0.78
Oct	0.83	0.91 0.82	0.14	0.96 0.84	0.07	0.96 0.84	0.93	0.89 0.79	0.87	0.90 0.81
Nov	-0.28	1.00 0.95	-0.44	1.00 0.91	0.19	0.94 0.89	0.35	0.92 0.88	0.23	0.94 0.88
Dec	-1.41	1.13 0.82	-1.90	1.18 0.85	-1.78	1.16 0.83	-1.69	1.15 0.84	-1.18	1.09 0.83

Table A.5: Monthly bias North Hecate.

Month	1 Pixel			3x3 Pixels			5x5 Pixels			6x6 Pixels			8x8 Pixels							
	Int.	Slope	r ²	N	Int.	Slope	r ²	N	Int.	Slope	r ²	N	Int.	Slope	r ²	N				
Jan	0.41	0.91	0.75	65	0.83	0.85	0.77	97	0.92	0.83	0.76	115	0.80	0.85	0.80	128	0.77	0.84	0.73	151
Feb	-0.22	1.00	0.86	93	-0.00	0.96	0.88	125	0.15	0.94	0.86	136	0.17	0.93	0.85	145	0.06	0.94	0.80	170
Mar	0.54	0.89	0.83	89	0.01	0.95	0.85	124	0.06	0.94	0.83	149	0.17	0.92	0.77	164	0.11	0.92	0.76	187
Apr	-0.31	0.98	0.79	103	-0.14	0.95	0.72	144	0.01	0.93	0.73	164	-0.15	0.95	0.76	177	-0.15	0.95	0.77	190
May	-0.10	0.95	0.75	123	-0.24	0.97	0.78	167	-0.32	0.97	0.76	190	-0.07	0.94	0.75	205	-0.13	0.95	0.73	219
Jun	0.01	0.96	0.78	85	-0.02	0.96	0.82	121	0.17	0.94	0.80	137	0.65	0.90	0.76	148	0.74	0.89	0.74	173
Jul	0.54	0.94	0.84	81	0.78	0.91	0.69	131	1.11	0.88	0.65	154	0.70	0.91	0.66	162	1.10	0.88	0.63	180
Aug	1.63	0.86	0.78	105	1.70	0.85	0.75	155	1.48	0.86	0.74	180	1.67	0.85	0.74	195	1.49	0.86	0.69	224
Sep	-0.32	1.01	0.84	109	-0.04	0.98	0.76	153	0.09	0.97	0.76	173	0.63	0.93	0.70	194	0.92	0.91	0.68	211
Oct	0.88	0.90	0.72	82	1.62	0.83	0.70	128	1.11	0.87	0.68	150	0.84	0.89	0.66	168	0.72	0.91	0.70	195
Nov	-0.16	1.00	0.83	69	-0.46	1.03	0.82	124	-0.45	1.02	0.78	145	-0.11	0.98	0.77	169	-0.03	0.97	0.78	192
Dec	0.79	0.89	0.87	64	1.12	0.84	0.82	98	1.11	0.84	0.83	113	1.01	0.85	0.81	124	0.77	0.87	0.80	144

Table A.6: Monthly bias La Perouse.

Month	1 Pixel			3x3 Pixels			5x5 Pixels			6x6 Pixels			8x8 Pixels							
	Int.	Slope	r ²	N	Int.	Slope	r ²	N	Int.	Slope	r ²	N	Int.	Slope	r ²	N				
Jan	3.70	0.53	0.43	102	2.97	0.61	0.49	137	2.76	0.63	0.53	165	2.65	0.64	0.55	172	2.74	0.63	0.54	186
Feb	-0.71	1.04	0.79	106	0.60	0.87	0.71	141	0.90	0.84	0.69	165	1.01	0.82	0.67	181	1.28	0.79	0.64	195
Mar	0.40	0.88	0.76	92	1.65	0.75	0.62	132	2.03	0.70	0.60	158	1.98	0.71	0.61	169	2.28	0.67	0.57	195
Apr	1.00	0.83	0.68	126	1.66	0.75	0.63	177	2.77	0.63	0.54	214	2.68	0.64	0.55	228	2.98	0.61	0.52	249
May	-0.26	0.97	0.90	124	0.11	0.94	0.80	187	0.02	0.94	0.80	222	0.75	0.88	0.75	231	0.79	0.87	0.72	256
Jun	0.52	0.93	0.85	118	0.64	0.92	0.83	169	0.31	0.94	0.82	203	0.47	0.93	0.81	213	0.65	0.91	0.80	236
Jul	2.09	0.82	0.69	178	1.86	0.83	0.66	258	1.90	0.83	0.66	299	1.94	0.83	0.65	314	2.19	0.81	0.64	346
Aug	1.51	0.86	0.73	138	1.97	0.83	0.73	233	2.60	0.78	0.66	278	2.82	0.77	0.66	296	3.14	0.75	0.61	327
Sep	0.83	0.90	0.81	168	1.10	0.88	0.78	261	1.38	0.86	0.76	303	1.49	0.85	0.76	315	1.95	0.82	0.73	336
Oct	1.33	0.86	0.79	127	0.58	0.92	0.81	182	0.58	0.92	0.80	226	0.67	0.91	0.79	237	0.65	0.91	0.76	262
Nov	-0.01	0.98	0.91	87	0.30	0.94	0.87	141	0.18	0.95	0.88	165	0.38	0.93	0.88	178	0.58	0.91	0.85	204
Dec	3.07	0.65	0.63	106	3.00	0.65	0.61	143	2.79	0.67	0.61	170	2.74	0.68	0.62	183	2.88	0.66	0.61	201

B SST climatology and anomaly for 2018-2019

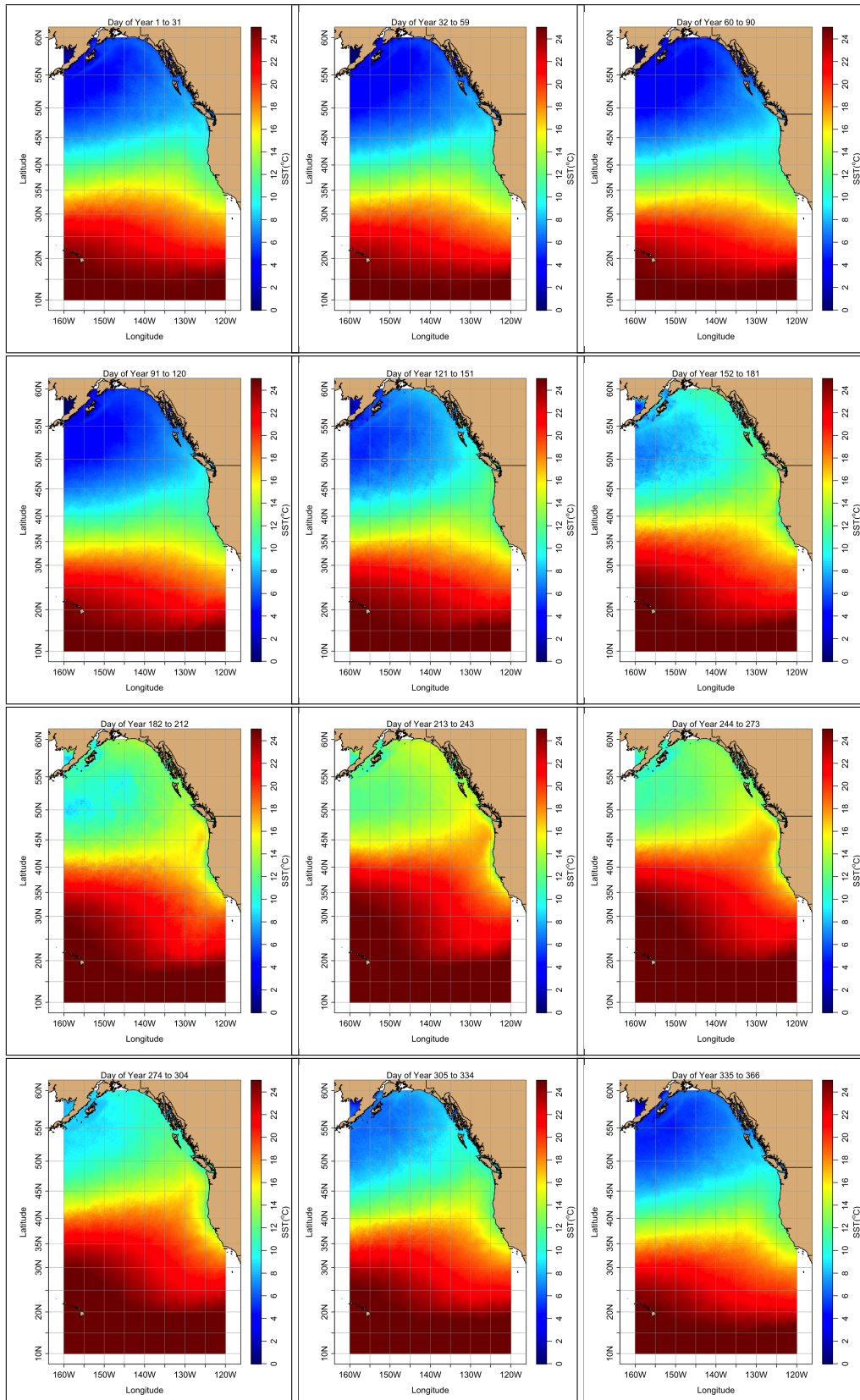


Figure B.1: Monthly climatology for SST from 1990 to 2003.

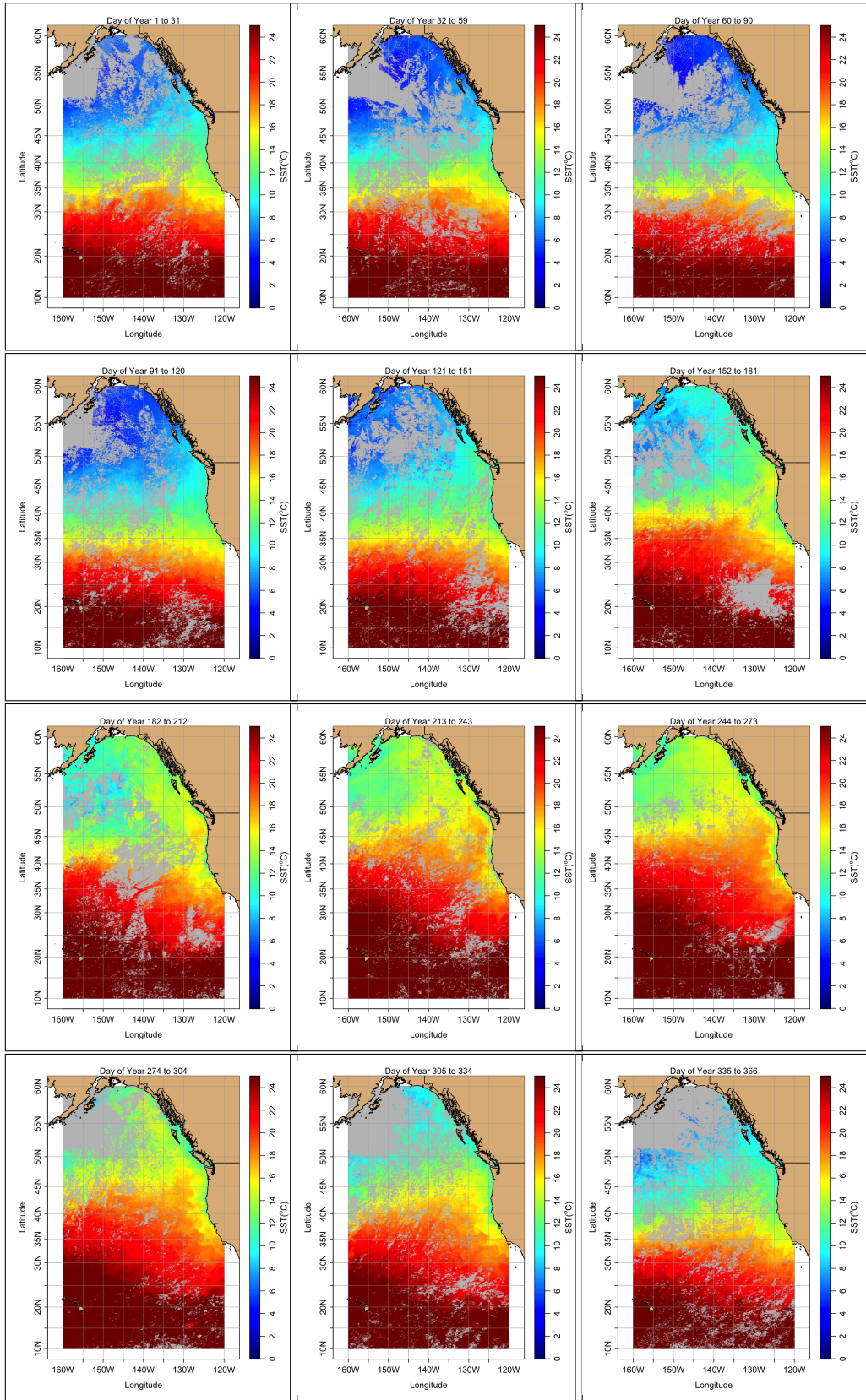


Figure B.2: Monthly composite for SST in 2018.

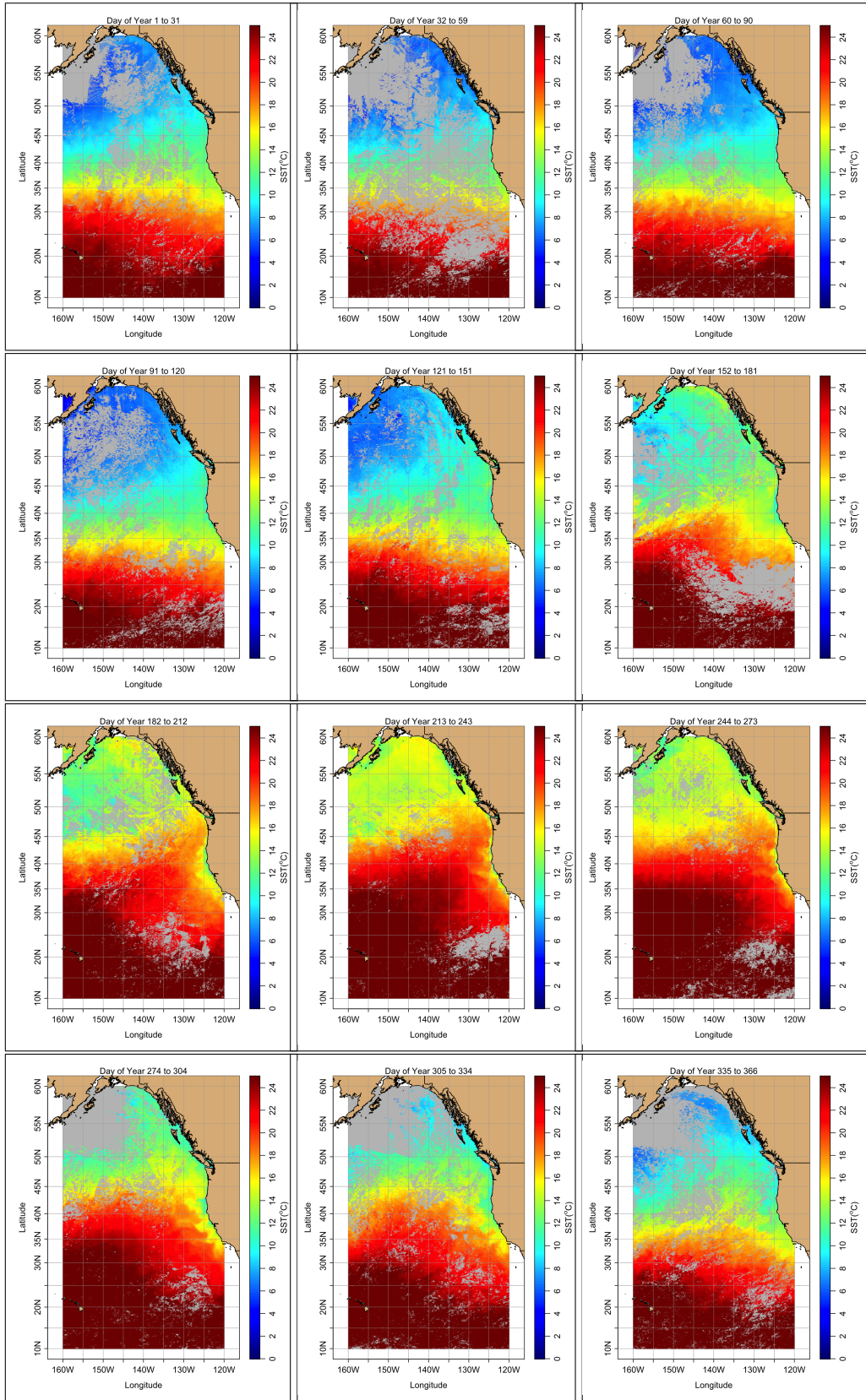


Figure B.3: Monthly composite for SST in 2019.

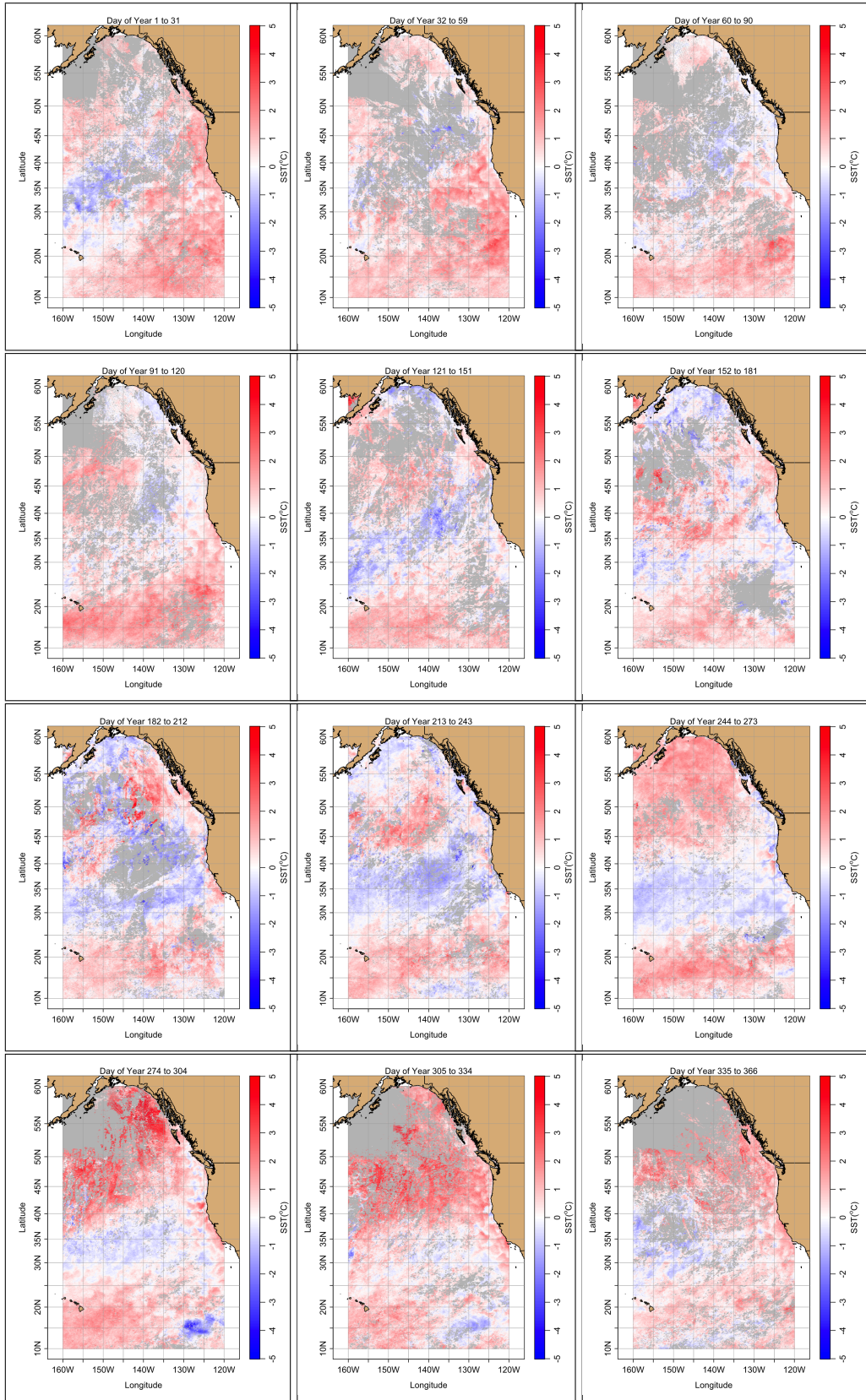


Figure B.4: Monthly comparison for SST in 2018.

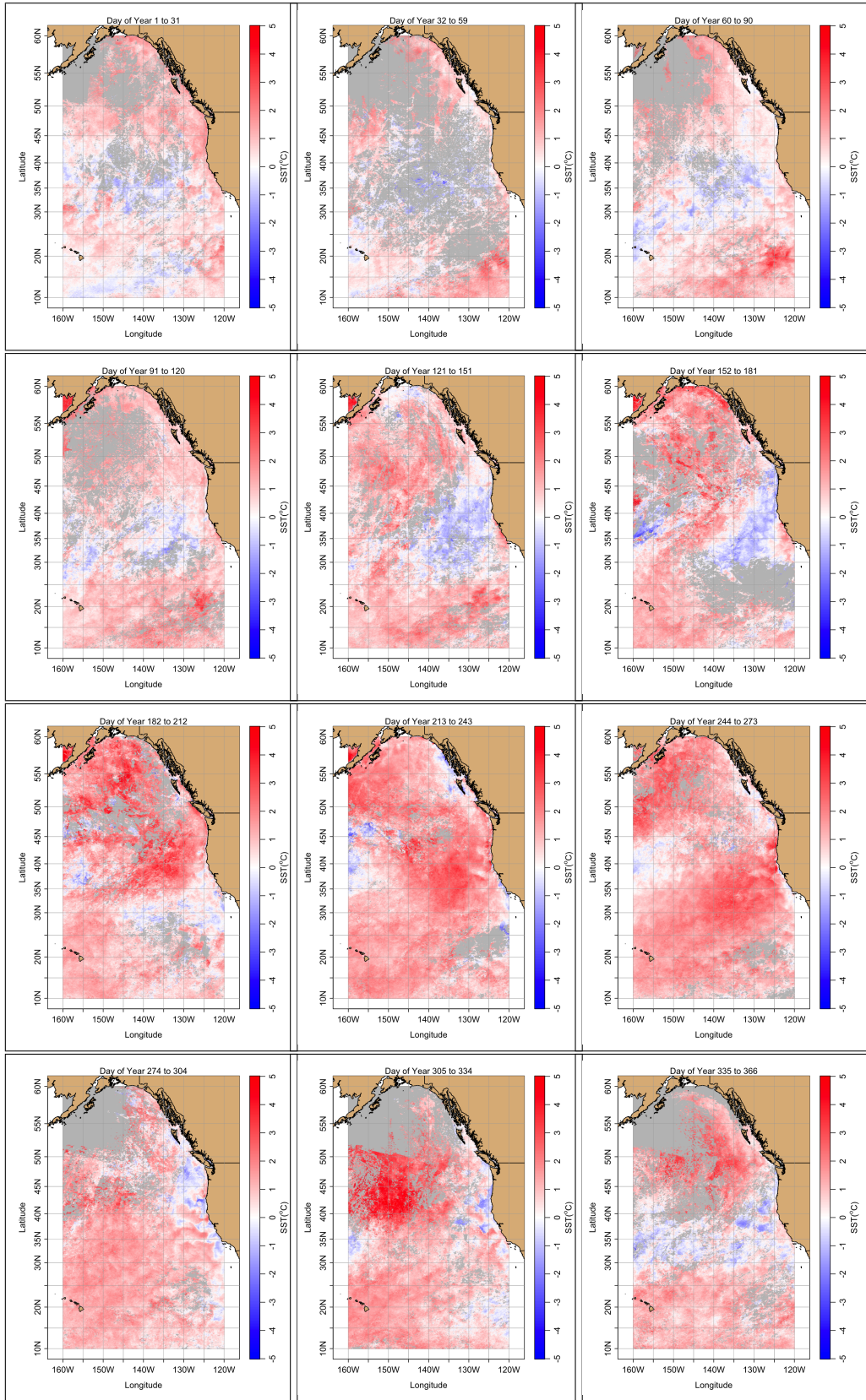


Figure B.5: Monthly comparison for SST in 2019.